Title
Heterogeneous chemistry in the troposphere: Experimental approaches and applications to the chemistry of sea salt particles

Journal
International Reviews in Physical Chemistry, 18(3)

ISSN
0144-235X

Authors
De Haan, David O
Brauers, Theo
Oum, Kawon
et al.

Publication Date
1999-07-01

DOI
10.1080/014423599229910

INTERNATIONAL REVIEWS IN PHYSICAL CHEMISTRY, 1999, VOL. 18, NO. 3, 343–385

Heterogeneous chemistry in the troposphere: experimental approaches and applications to the chemistry of sea salt particles

DAVID O. DE HAAN†, THEO BRAUERS‡, KAWON OUM§, JOCHEN STUTZ‖, TRENT NORDMEYER¶ and BARBARA J. FINLAYSON-PITTS††

Department of Chemistry, University of California, Irvine, California 92697-2025, USA

Halogen atoms, particularly chlorine atoms, are well known to be highly reactive and to play a central role in the chemistry of the upper atmosphere. A large potential source of these halogens in the lower atmosphere (troposphere) exists in the form of sea salt particles. A variety of laboratory, field and modelling studies strongly suggests that there are heterogeneous reactions of sea salt particles which generate photochemically active halogen species such as Cl_2 in marine areas. In addition, there is increasing evidence for a contribution of bromine atoms to tropospheric chemistry in marine regions at high latitudes. We review here briefly the potential importance of such halogen reactions and evidence for their role in the chemistry of the troposphere. Studies carried out in this laboratory to elucidate, at a molecular level, the mechanisms of reaction of synthetic sea salt and its components with gases of tropospheric interest are reviewed. Initial results obtained using a new aerosol apparatus recently constructed in this laboratory to study the reactions of aerosol particles above and below the deliquescence point of the salts are also discussed.

1. Introduction

It has been recognized for many decades that gas, liquid and solid phases all play a role in atmospheric chemistry (Leighton 1961, Andreae and Crutzen 1997, Finlayson-Pitts and Pitts 1997, Ravishankara 1997). While the overall reactions occurring in the gas phase are reasonably well understood, much less is known about reactions involving gases at surfaces, at either the gas–solid interface or the gas–liquid interface. Such reactions are generally referred to as 'heterogeneous' in the context of atmospheric chemistry. While the details of such processes at the molecular level are not well understood, they are critical for quantifying their role in the chemistry of the atmosphere, and incorporating this chemistry into models of photochemical air pollution, acid deposition and global climate change.

† Present address: Department of Chemistry and Biology, Lyon College, PO Box 2317, 2300 Highland Road, Batesville, Arkansas 72503-2317, USA.

‡ Present address: Institut für Atmosphärische Chemie, Forschungszentrum KFA, Jülich, Germany.

§ Present address: Institut für Physikalische Chemie, Universität Göttingen, Tammannstrasse 6, D-37077 Göttingen, Germany.

‖ Present address: Institut für Umweltphysik, Im Neuenheimer Feld 366, D-69120 Heidelberg, Germany.

¶ Present address: Department of Chemistry, University of Wisconsin-Stout, PO Box 790, Menomonie, Wisconsin 54751-0790, USA.

†† Author for correspondence. Tel.: (949) 824-7670; Fax (949) 824-3168; Email: bjfinlay@uci.edu.

International Reviews in Physical Chemistry ISSN 0144-235X print/ISSN 1366-591X online © 1999 Taylor & Francis Ltd
http://www.tandf.co.uk/JNLS/rpc.htm http://www.taylorandfrancis.com/JNLS/rpc.htm

Historically, studies of heterogeneous reactions of atmospheric interest have been difficult to address experimentally owing to the conflicting demands of ultrahigh-vacuum techniques used in surface science and the high-pressure high-water-vapour conditions relevant to the atmosphere (Hemminger 1999). However, with the discovery that chemistry on and in polar stratospheric clouds was driving Antarctic ozone depletion (see World Meteorological Organization (1995) for a review), this area of heterogeneous chemistry has been attacked with renewed vigour. Most recently, increased attention has been paid to reactions of gases at liquid and solid interfaces relevant to the troposphere (Ravishankara 1997).

In this article, we emphasize the understanding of heterogeneous tropospheric reactions at a molecular level in order to extrapolate reliably to atmospheric conditions. We shall use as the central example reactions of sea salt particles and their components, both solid and aqueous. As discussed in more detail in the following section, interest in the reactions of sea salt particles stems from their potential to act as sources of halogen atoms in the troposphere. In this context, we describe a variety of experimental approaches, including a new aerosol chamber recently constructed in this laboratory which was designed to study such gas–particle interactions under conditions simulating those found in the troposphere.

In order to place the potential importance of the heterogeneous chemistry of sea salt particles in perspective, we first briefly review some relevant gas-phase chemistry of organics and oxides of nitrogen in the troposphere, as well as some of the evidence from field studies which point to gas-phase halogen chemistry as also being important at the Earth's surface in marine areas.

1.1. *Gas-phase tropospheric chemistry*

The major gas-phase species driving the chemistry of both polluted and remote regions are known to include the hydroxyl-free radical (OH) during the day, the nitrate radical (NO_3) at night, and ozone (O_3) both day and night. The different times of day at which each of these species is important reflect their sources and sinks. For example, the major sources of OH are photochemical, such as the photolysis of O_3, nitrous acid or HCHO and other carbonyl compounds:

$$O_3 + h\nu \rightarrow O(^1D) + O_2 \quad (1)$$

$$O(^1D) + H_2O \rightarrow 2OH \quad (2)$$

$$\xrightarrow{M} O(^3P), \quad (3)$$

$$HONO + h\nu \rightarrow OH + NO, \quad (4)$$

$$HCHO + h\nu \rightarrow H + HCO, \quad (5)$$

$$H + O_2 \xrightarrow{M} HO_2, \quad (6)$$

$$HCO + O_2 \rightarrow HO_2 + CO, \quad (7)$$

$$HO_2 + NO \rightarrow OH + NO_2. \quad (8)$$

An additional source of OH is from ozone–alkene reactions (for example Atkinson *et al.* (1992), Paulson and Orlando (1996), Paulson *et al.* (1997) and Donahue *et al.* (1998)), where decomposition of the Criegee intermediate can generate OH in significant yields (up to 100%), depending on the structure of the parent alkene. Although there are some free radical mechanisms which can generate OH in the dark such as those initiated by the decomposition of peroxyacetyl nitrate (PAN) (Finlayson-Pitts and Pitts 1986) and the oxidation of organics by NO_3 (Platt *et al.* 1990, Aliwell and Jones 1998), these produce much smaller concentrations of OH at night than the

various photolytic sources generate during the day. As a result, OH typically peaks at midday at concentrations in the approximate range 10^6–10^7 radicals cm^{-3}, and nighttime concentrations are of the order of 10^4 cm^{-3} or less (for example Eisele *et al.* (1994), Dorn *et al.* (1996) and Hofzumahaus *et al.* (1996)).

The nitrate radical is formed by the reaction of NO_2 with O_3:

$$NO_2 + O_3 \rightarrow NO_3 + O_2. \tag{9}$$

Because NO_3 absorbs light in the visible region from about 570 to 670 nm (De More *et al.* 1997), it rapidly photolyses at dawn and its reactions are therefore only important in the dark.

Ozone is formed by the reaction of ground-state oxygen atoms $O(^3P)$ generated by NO_2 photolysis, with O_2:

$$NO_2 + h\nu(\lambda < 420 \text{ nm}) \rightarrow NO + O(^3P), \tag{10}$$

$$O(^3P) + O_2 \xrightarrow{M} O_3. \tag{11}$$

NO also reacts rapidly with O_3:

$$NO + O_3 \rightarrow NO_2 + O_2; \tag{12}$$

therefore high concentrations of NO and O_3 do not coexist. Reactions (10)–(12) are in effect a null cycle. However, NO is also converted to NO_2 through reaction (8) of HO_2 and, as seen below, through reactions involving organic peroxy free radicals, ultimately leading to net ozone formation.

Because most NO_2 in the troposphere is formed from the atmospheric oxidation of NO emitted by combustion processes, there is a delay between the emissions of NO and organics (which, as discussed shortly, play a key role in the $NO \rightarrow NO_2$ conversion), and the formation of O_3. As a result, ozone concentrations in polluted areas generally peak at midday and later. Some tropospheric ozone also results from stratospheric intrusions (Holton *et al.* 1995). Ozone is removed by photolysis (reaction (1) above) and by reactions such as those with alkenes, as well as by deposition at the surface, but these are sufficiently slow that significant concentrations of ozone can exist both day and night.

In both polluted and remote areas, ozone formation chemistry is essentially a chain process involving volatile organic compounds and oxides of nitrogen ($NO_x = NO + NO_2$). Using ethane as an example, OH initiates the oxidation, which in the presence of sufficient NO (about 10–50 ppt), ultimately leads to ozone formation:

$$OH + C_2H_6 \rightarrow H_2O + C_2H_5, \tag{13}$$

$$C_2H_5 + O_2 \xrightarrow{M} C_2H_5O_2, \tag{14}$$

$$C_2H_5O_2 + NO \rightarrow NO_2 + C_2H_5O, \tag{15}$$

$$C_2H_5O + O_2 \rightarrow CH_3CHO + HO_2, \tag{16}$$

followed by reactions (8), (10) and (11) above to generate O_3. The acetaldehyde formed also generates HO_2 through its subsequent oxidation (e.g. by OH) and by photolysis, analogous to steps (5)–(7).

Oxides of nitrogen are important components of this cycle. NO is first oxidized to

NO_2, which is then either photolysed (reaction (10)) or oxidized to other oxides of nitrogen such as HNO_3, according to

$$OH + NO_2 \xrightarrow{M} HNO_3, \tag{17}$$

or N_2O_5, according to

$$NO_2 + NO_3 \leftrightarrow N_2O_5. \tag{18}$$

N_2O_5 rapidly hydrolyses on particle and other surfaces in the atmosphere, forming HNO_3:

$$N_2O_5 + H_2O \xrightarrow{\text{surface}} 2HNO_3. \tag{19}$$

At low NO levels, the alkyl peroxy and hydroperoxyl free radicals primarily react with each other instead of with NO, limiting the chain oxidation of NO and the generation of ozone.

The interest in sea salt chemistry stems from the potential for photochemically active halogen compounds to be formed from its reactions in the troposphere (Cicerone 1981, Finlayson-Pitts 1993, Graedel and Keene 1995, Keene 1995, Keene *et al.* 1996). Such photochemically labile compounds can absorb light to generate halogen atoms. Chlorine atoms are particularly reactive, with rate constants for all but the smallest alkanes being near the collision-controlled limit (Atkinson 1997). The chlorine atom reaction with ethane, for example, occurs with a rate constant at 298 K of 5.7×10^{-11} cm^3 $molecule^{-1}$ s^{-1}, two orders of magnitude faster than the OH–ethane reaction. As a result, if present in the troposphere at concentrations even one or two orders of magnitude less than OH, chlorine atoms could play a significant role in initiating organic oxidation:

$$Cl + C_2H_6 \rightarrow HCl + C_2H_5. \tag{20}$$

Subsequent reactions of the alkyl radical to produce ozone have been summarized above. Chlorine atoms may also play an important role in the oxidation of species such as dimethyl sulphide (Keene *et al.* 1996).

Table 1 shows typical peak concentrations of OH, O_3, NO_3 and chlorine atoms, and the times of day that these peak concentrations generally occur for each. Also shown are the rate constants for their reactions with some typical organics found in the troposphere, and the calculated lifetimes of these organics with respect to reaction with each species. Note that the peak OH concentration cited in table 1 typically occurs around midday; at dawn when chlorine atoms are expected to peak, the OH concentration is about an order of magnitude smaller than the peak cited in table 1, and the lifetimes of organics with respect to removal by OH correspondingly longer. Clearly, chlorine atoms may be a major contributor to initiating organic oxidation at dawn in the marine boundary layer, which includes many coastal urban areas.

While many measurements of OH, O_3 and NO_3 have been made world-wide under a variety of conditions, there is none to date of atomic chlorine in the troposphere. The value in table 1 is an estimate, based on a combination of modelling and field studies in which the concentration has been derived indirectly from changes in the concentrations of organics with which chlorine atoms react, and from recently measured concentrations of Cl_2 in the marine boundary layer (see discussion below).

Bromine atoms also react with some organics such as HCHO, but the reactions with many species such as alkanes are very slow at room temperature. The molar ratio of bromide to chloride in sea salt, expected to be the major source of tropospheric

Table 1. Typical peak concentrations and times for species responsible for oxidizing organics in the troposphere, and calculated lifetimes with respect to these reactions.

Species	Typical peak concentration (number cm^{-3})	Typical time of peak	Organic	$k^{298\ K}$ [a] (cm^3 molecules^{-1} s^{-1})	Lifetime τ [b]
OH	1×10^{7} [c]	Midday	C_3H_8	1.1×10^{-12}	25 h
			C_3H_6	2.6×10^{-11} [f]	1.1 h
			HCHO	1.0×10^{-11}	2.8 h
			CH_3SCH_3	5.0×10^{-12}	5.6 h
O_3	$(2.5–7.5)\times10^{12}$ [d] (0.1–0.3 ppm)	Midday to late afternoon	C_3H_6	1.0×10^{-17} [f]	3–10 h
NO_3	1.0×10^{9} [e] (40 ppt)	Night-time	C_3H_8	1.7×10^{-17} [f]	2 years
			C_3H_6	9.5×10^{-15} [f]	29 h
			HCHO	5.8×10^{-16}	20 days
			CH_3SCH_3	1.0×10^{-12}	0.3 h
Cl	1×10^{5} [g]	Dawn	C_3H_8	1.4×10^{-10}	20 h
			C_3H_6	2.3×10^{-10} [h]	12 h
			HCHO	7.3×10^{-11}	38 h
			CH_3SCH_3	4.2×10^{-10}	6.6 h

[a] From De More *et al.* (1997) unless otherwise specified.
[b] $\tau = 1/k[X]$ where X = OH, O_3, NO_3 or Cl respectively.
[c] From Eisele *et al.* (1994), Dorn *et al.* (1996) and Hofzumahaus *et al.* (1996).
[d] Typical values for urban–rural to highly polluted (Finlayson-Pitts and Pitts 1986).
[e] From Platt (1994).
[f] From Atkinson (1997).
[g] Estimated for the marine boundary layer; see text.
[h] From Stutz *et al.* (1998).

halogens, is about 1:650 so that there is substantially less bromine available to play a role in tropospheric chemistry. However, because of its relatively slow reactions with most organics, it is not removed as rapidly from the troposphere as are chlorine atoms, and hence a relatively larger fraction reacts with O_3. In addition, as discussed in more detail below, there are autocatalytic cycles for regenerating photochemically active bromine in the troposphere. As a result, it is believed that there are circumstances where bromine plays a significant role in tropospheric chemistry, especially in high-latitude marine regions.

It is well known that both chlorine and bromine atoms also react with O_3 in the stratosphere, and this can occur in the troposphere as well:

$$Cl + O_3 \rightarrow ClO + O_2, \tag{21}$$

$$Br + O_3 \rightarrow BrO + O_2. \tag{22}$$

Subsequent reactions of ClO and BrO (see below) can regenerate the atomic halogens (Wayne *et al.* 1995). Thus, depending on the relative concentrations of O_3 and the organics, the halogens may contribute to either ozone destruction or ozone formation.

In addition to salt particles generated by wave action which can be carried inland significant distances (Shaw 1991), there are other episodic sources of salt in the troposphere which are expected to react in a manner similar to sea salt particles in the marine boundary layer and coastal regions. For example, the smoke plume formed during the burning of oil wells in Kuwait contained significant salt concentrations

owing to the presence of brine mixed with the oil (for example Cahill *et al.* (1992), Cofer *et al.* (1992), Daum *et al.* (1993), Ferek *et al.* (1992), Parungo *et al.* (1992), Sheridan *et al.* (1992), Stevens *et al.* (1993) and Lowenthal *et al.* (1993)). Some volcanic eruptions which are alkaline in nature, such as that of El Chichon, generate a brief pulse of salt emissions (Woods and Chuan 1983, Woods *et al.* 1985), which have been proposed to play a role in the stratosphere immediately after the eruptions (Michelangeli *et al.* 1991). There are also salt flats and inland alkaline bodies of water such as the Dead Sea in Israel (Hebestreit *et al.* 1998) and the Salton Sea in California, USA, where salt-containing particles can be generated by wind action and erosion of dried salt crusts at the lake edges (Reid *et al.* 1994).

1.2. *Evidence from field studies for gas-phase photolysable chlorine compounds*

A number of field studies also suggest the presence of photolysable chlorine compounds in marine areas. For example, Keene *et al.* (1993) and Pszenny *et al.* (1993) developed a mist chamber technique to differentiate HCl from other chlorine gases in a coastal area and reported the formation of up to about 125 ppt expressed as Cl_2 (but not specifically identified as Cl_2) in the dark. While the concentrations decreased at dawn, they did not fall to zero as expected for Cl_2, suggesting the presence of other compounds such as HOCl. In contrast, over an inland area in eastern North America, HCl appears to be the major gaseous chlorine-containing species (Maben *et al.* 1995).

Recently, Spicer *et al.* (1998) used atmospheric pressure ionization tandem mass spectrometry (API–MS) to identify and measure Cl_2 for the first time in a marine area. The peak levels at night were similar to those observed by Pszenny *et al.* (1993), about 150 ppt, and decreased below the detection limit at dawn. Modelling studies using a box model indicate that these Cl_2 concentrations are much greater than can be produced by the reactions between salt aerosol and oxides of nitrogen described below. Indeed, the nature of the reaction(s) producing these concentrations remains unknown.

There have also been indirect studies which have inferred chlorine atom concentrations in the marine boundary layer from the concentrations of organics which react with Cl as well as OH (for example Wingenter *et al.* (1996) and Singh *et al.* (1996a)). While peak concentrations in the range 10^4–10^6 chlorine cm^{-3} are derived from such measurements, the atomic chlorine concentration averaged over the entire troposphere and over time is, as expected, much smaller. Tetrachloroethene has been used as a probe for global tropospheric Cl, since it reacts relatively rapidly with Cl compared with OH. The global concentrations of this compound are consistent with its known emissions and removal solely by OH, from which an upper limit to the *annually* and *globally averaged* tropospheric chlorine atom concentration of less than 10^3 atoms cm^{-3} has been derived (Singh *et al.* 1996b, Rudolph *et al.* 1996). Assuming that most of it is in the marine boundary layer closest to the ocean surface, these studies give an upper limit to the annually averaged concentration in the marine boundary layer of less than $(5\text{–}15) \times 10^3$ atoms cm^{-3} (Singh *et al.* 1996b), corresponding to daytime concentrations of less than $(0.5\text{–}3) \times 10^4$ atoms cm^{-3}. Such estimates may not be inconsistent with *peak* concentrations of 10^4–10^6 atoms cm^{-3} at dawn.

In short, the available evidence suggests that chlorine atom chemistry should be most important in marine areas close to the Earth's surface where its source in the form of sea salt is abundant. There are clearly some unknown reactions generating significant quantities of Cl_2 and perhaps other chlorine atom precursors as well in this

region. Depending on the nature of these reactions and the concentrations of chlorine atoms generated by them (suggested to peak at about 10^5 atoms cm^{-3} at dawn (Pszenny *et al.* 1993, Spicer *et al.* 1998)), they could play a significant role in the boundary layer chemistry of many organics, including in coastal urban areas.

1.3. *The Arctic at polar sunrise: evidence for gaseous bromine and chlorine chemistry*

In the mid-1980s, a surprising phenomenon was reported from ground-based measurements. Ozone at the surface was rapidly depleted in April at polar sunrise, over time periods of hours to days (Bottenheim *et al.* 1986, 1990, Oltmans and Komhyr 1986, Barrie *et al.* 1988). The removal is quite extensive both horizontally and vertically. For example, Solberg *et al.* (1996) reported episodes in the Norwegian Arctic in which O_3 was almost depleted from the surface to an altitude of about 2 km. Elemental analysis of particles collected on filters showed an anticorrelation between ozone and filter bromide, which could be due to bromide in particles and/or possibly to gaseous HBr being taken out on the filter (Barrie *et al.* 1988). This relationship suggested that the ozone destruction was due to the formation and reaction of gaseous bromine atoms, for example

$$Br + O_3 \rightarrow BrO + O_2, \tag{22}$$

$$BrO + BrO \rightarrow 2Br + O_2. \tag{23}$$

Various mechanisms for activation of bromine under Arctic conditions have been hypothesized (see Niki and Becker (1993) for a summary). McConnell *et al.* (1992), for example, proposed that HBr and organic compounds containing bromine would be adsorbed on ice crystals and airborne particles and subsequently converted to Br_2. Fan and Jacob (1992) proposed that this conversion occurred through reaction in aerosols of HOBr with HBr:

$$HOBr + Br^- + H^+ \leftrightarrow Br_2 + H_2O. \tag{24}$$

HOBr can be formed in the gas phase through the reaction of BrO with HO_2:

$$BrO + HO_2 \rightarrow HOBr + O_2; \tag{25}$$

subsequently it is taken up into aerosol particles. Alternatively, it can be formed on or in the particles by hydrolysis of $BrONO_2$:

$$BrONO_2 + H_2O \xrightarrow{\text{particles}} HOBr + HNO_3. \tag{26}$$

However, there is insufficient airborne particulate bromide to cause the observed ozone destruction, even if all particulate bromide is converted to active forms by these reactions. Tang and McConnell (1996) proposed that the major mechanism for conversion of HOBr back to Br_2 involved sea salt particles deposited on the snow pack, with the chain reaction initiated by photolysis of a 'seed' source of bromine atoms such as $CHBr_3$.

There is evidence from field studies for the presence of both bromine and chlorine atom precursors. For example, Impey *et al.* (1997) have shown that there are compounds present before and during Arctic sunrise which photolyse to generate atomic chlorine and bromine respectively. The concentrations of these precursors are up to 100 ppt expressed as Cl_2 and 38 ppt expressed as Br_2. However, the exact nature of these halogen atom precursors is not known.

The concentrations of chlorine and bromine atoms during these episodes have been estimated by a number of researchers. Chlorine atoms have been estimated to be

in the range from mid-10^3 to 10^5 atoms cm^{-3}, with bromine atoms about two to three orders of magnitude larger (for example Jobson *et al.* (1994), Ariya *et al.* (1996), Impey *et al.* (1997)).

As discussed in more detail in section 2.2, Sander and Crutzen (1996) and Vogt *et al.* (1996a) have proposed autocatalytic cycles for the reactions of sea salt particles at midlatitudes which generate photochemically active halogen gases such as BrCl, Br_2 and Cl_2, and it is likely that these also occur in the Arctic.

A key intermediate in this ozone destruction cycle is BrO, which can be detected by differential optical absorption spectrometry (DOAS). Platt and Hausmann (1994) and Tuckermann *et al.* (1997) have measured BrO at levels up to 30 ppt using DOAS at polar sunrise, confirming the role of bromine in the ozone destruction. In addition, tropospheric column BrO concentrations in the Arctic have been extracted using satellite measurements (for example Richter *et al.* (1998), Chance (1998) and Wagner and Platt (1998)). Tropospheric BrO is enhanced from February to May over a large region of the Arctic, including most of Hudson Bay and along the coast line of the Arctic Ocean. The BrO appears to be coincident with the sunlight intensity increase and the retreat of sea ice.

However, despite the likelihood of chain reactions which regenerate Br and BrO, the initiation step remains to be elucidated. As discussed in more detail below, recent work in this and other laboratories strongly suggests that this initiation step involves the oxidation of bromide ion by O_3 in the dark to form Br_2, which then photolyses to bromine atoms at dawn.

2. Heterogeneous sea salt reactions in the troposphere

There are a number of laboratory, field and modelling studies which point to the heterogeneous reactions of sea salt particles as the source of gas-phase halogens described above. We briefly summarize these in the following sections before describing some of the research from this laboratory which is designed to understand these processes at a molecular level.

2.1. *Halogen deficiencies in sea salt particles*

Wave action in marine areas generates small airborne droplets of seawater (Woodcock 1953, 1972, Blanchard 1985, Gong *et al.* 1997a, b, O'Dowd *et al.* 1997). Under many circumstances in marine areas, the particles exist as concentrated aqueous solutions since the deliquescence point at 298 K is about 75% relative humidity (Tang *et al.* 1977, 1978, 1997, Tang and Munkelwitz 1984, 1993). However, as they are carried inland or to higher altitudes (Ikegami *et al.* 1994), the water can evaporate, leaving a suspended particle consisting of the solids which were in the sea water. Therefore, reactions of both solids and aqueous phase particles must be considered.

While the particles formed by wave action should have an ionic composition reflecting the sea-water source, it has been known for at least four decades that such particles are often deficient in chloride and bromide relative to sodium (for example Junge (1956), Moyers and Duce (1972), Keene *et al.* (1990), Mouri and Okada (1993) and McInnes *et al.* (1994)). This suggests sea salt particles react with atmospheric gases such as acids (HNO_3 and H_2SO_4), oxides of nitrogen or other oxidants, converting condensed-phase halides into gas-phase halogen species. Indeed, $NaNO_3$ and Na_2SO_4 have been observed in sea salt aerosols using transmission electron microscopy with

energy-dispersive X-ray spectrometry (Pósfai *et al.* 1995). Some possible reactions are discussed in the following sections.

2.2. *Laboratory and modelling studies of heterogeneous reactions of potential importance*

Field observations of halogen deficits in marine regions as well as the observation of excess nitrate and/or sulphate in the particles have been attributed to ion exchange reactions with nitric and sulphuric acids:

$$NaCl_{(cond)} + HNO_{3(g)} \rightarrow HCl_{(g)} + NaNO_{3(cond)}\ , \tag{27}$$

$$2NaCl_{(cond)} + H_2SO_{4(g,\ aq)} \rightarrow 2HCl_{(g)} + Na_2SO_{4(cond)}\ . \tag{28}$$

The NaCl is in the condensed phase (shown as cond), which can be either solid or aqueous, depending on the relative humidity. HNO_3 is in the gas phase and, as discussed in the following, HCl will be degassed from aqueous particles if they become sufficiently acidic.

The attribution of observed halogen deficits to reactions (27) and (28) is based both on well known bulk-phase chemistry as well as more atmospherically relevant studies of NaCl aerosol particle reactions with NO_2 in humid air (Robbins *et al.* 1959, Cadle and Robbins 1960). In the latter studies, the measured loss of chloride from NaCl particles and the formation of nitrate was attributed to the formation of HNO_3 from NO_2, followed by reaction (27). Subsequent studies of the HNO_3 reaction discussed in more detail below and in the article in this issue by Hemminger (1999) have elucidated many of the details of the kinetics and mechanism of the reaction of HNO_3 with solid NaCl (Fenter *et al.*, 1994, 1996, Vogt and Finlayson-Pitts 1994a, b, 1995a, Laux *et al.* 1994, Leu *et al.* 1995, Beichert and Finlayson-Pitts 1996, Vogt *et al.* 1996b).

Some studies in coastal urban regions have correlated halogen deficiencies in sea salt particles with the presence of anthropogenic pollutants such as oxides of nitrogen (for example Martens *et al.* (1973)). However, halogen deficiencies have also been observed in particles collected over the North Atlantic and, in this case, the excess sulphate and nitrate measured in the particles only accounted for about 40% of the missing chloride (Keene *et al.* 1990). This suggests that reactions other than those of nitric and sulphuric acids may generate gaseous halogen species.

Another important factor with respect to reactions (27) and (28) is that sea water is initially slightly basic, with a pH of about 8. The thermodynamics of HCl partitioning between gas and solution are well known and, at this pH, HCl is not expected to degas from solution (Brimblecombe and Clegg 1988, Clegg and Brimblecombe 1990). As a result, significant chloride deficits are not anticipated in such particles until they are acidified. However, through uptake and reactions of gases such as SO_2 (Chameides and Stelson 1992, Sievering *et al.* 1992, 1995, O'Dowd *et al.* 1997, Keene *et al.* 1998a, b), sea salt particles can be quite acidic. For example, Keene and Savoie (1998) have estimated pH values in the range from about 2.5 to 3.5 in deliquesced sea salt particles in Bermuda.

HCl, a product of the ion exchange reactions of nitric and sulphuric acids in the troposphere, is relatively unreactive. The reaction of HCl with OH is sufficiently slow ($k^{298} = 8.0 \times 10^{-13}$ cm^3 molecule^{-1} s^{-1} (De More *et al.* 1997)) that the lifetime ($\tau = 1/k[OH]$) of HCl with respect to this reaction is 14 days at an OH concentration of 1×10^6 radicals cm^{-3}. However, HCl is quite soluble, so that it is readily removed by deposition processes. As a result, reactions (27) and (28) alone followed by the

OH+HCl reaction are not predicted to generate sufficient concentrations of tropospheric chlorine atoms to play a significant role in tropospheric chemistry (Singh and Kasting 1988).

Schroeder and Urone (1974) reported that NO_2 at high (about 10 Torr) concentrations reacted with NaCl to form nitrosyl chloride, according to

$$2NO_2(g) + NaCl(s) \rightarrow ClNO(g) + NaNO_3(s), \quad (29)$$

and suggested that photolysis of the ClNO product would generate chlorine atoms in the troposphere. $NaNO_3$ was subsequently identified as the solid product by Chung *et al.* (1978), and reaction (29) was shown to occur at least down to the parts per million range (Finlayson-Pitts, 1983). A variety of studies have been carried out to define the reaction kinetics and elucidate the mechanism (Sverdrup and Kuhlman 1980, Zetzsch 1987, Zetzsch *et al.* 1988, Mamane and Gottlieb 1990, Winkler *et al.* 1991, Behnke *et al.* 1993a, b, Vogt and Finlayson-Pitts 1994a, b, Karlsson and Ljungström 1995, Peters and Ewing 1996). Several of these show that the reaction is second order with respect to NO_2 (Vogt and Finlayson-Pitts 1994a, b, Peters and Ewing 1996), although more complex behaviour was observed by Winkler *et al.* (1991), who reported a dependence on the square root of the NO_2 concentration. Second-order kinetics may reflect either a multistep oxidation mechanism or that the reactant is the dimer of NO_2, that is N_2O_4. Assuming that N_2O_4 is the reactant, the reaction probability γ, defined as the fraction of reactions of the gas with the surface that lead to collision, for a N_2O_4–NaCl reaction is approximately 10^{-4} for NaCl powders (Vogt and Finlayson-Pitts 1994a, b). Peters and Ewing (1996) reported a γ value of $(1.3 \pm 0.3) \times 10^{-6}$ using single-crystal NaCl cleaved along the (100) face. However, this increased to 1.1×10^{-4} in the presence of water vapour at 9.5 mbar. At any rate, given the small concentrations of N_2O_4 which will coexist with NO_2 at the sub-parts per million concentrations found in ambient air even in polluted regions, it is unlikely that this reaction of NO_2–N_2O_4 will be important in the troposphere.

Subsequent studies in this and other laboratories (Finlayson-Pitts *et al.* 1989a, Behnke and Zetzsch 1989a, b, 1990, Behnke *et al.* 1991, 1992, 1993a, b, 1994, 1995, 1997, Livingston and Finlayson-Pitts 1991, Junkermann and Ibusuki 1992, Zetzsch and Behnke 1992, 1993, Niki and Becker 1993, George *et al.* 1994, Msibi *et al.* 1994, Timonen *et al.* 1994, Vogt and Finlayson-Pitts 1994a, b, 1995a, Caloz *et al.* 1996, Fenter *et al.* 1996, Schweitzer *et al.* 1998) established that, in addition to the HNO_3 and NO_2 reactions, there were additional processes involving other oxides of nitrogen which could also generate photochemically active compounds, for example

$$NaCl(s) + N_2O_5(g) \rightarrow ClNO_2(g) + NaNO_3(s), \quad (30)$$

$$NaCl(s) + ClONO_2(g) \rightarrow Cl_2(g) + NaNO_3(s). \quad (31)$$

Chlorine nitrate, thought to be a major reservoir of active chlorine in the troposphere (Singh and Kasting 1988), is formed by the reaction of ClO with NO_2:

$$ClO + NO_2 \xrightarrow{M} ClONO_2. \quad (32)$$

Reactions (30) and (31) are similar to the low-temperature reactions in which these gases react with HCl–ice present in polar stratospheric clouds (see World Meteorological Organization (1995) for a review). Analogous reactions of NaBr and KBr to give photolysable bromine species also occur at room temperature (for example Finlayson-Pitts and Johnson (1988), Finlayson-Pitts *et al.* (1989b, 1990), Sturges

(1989), Berko *et al.* (1991), Behnke *et al.* (1994), Caloz *et al.* (1996), Fenter *et al.* (1996), Leu *et al.* (1997), Frenzel *et al.* (1998) and Mochida *et al.* (1998)).

The nitrate radical has also been shown recently to react with NaCl and KBr (Seisel *et al.* 1997). While measuring atoms is very difficult in such studies, Seisel *et al.* reported evidence that chlorine and bromine atoms are the primary products in these reactions.

In addition to these reactions of oxides of nitrogen, there were some intriguing indications from aerosol chamber studies of Zetzsch and Behnke (1993) and Behnke *et al.* (1995) that reactions of O_3 with aqueous sea salt particles might lead to the generation of photochemically active chlorine compounds. Dry NaCl does not react at a significant rate with O_3 (Alebic-Juretic *et al.* 1992). However, photolysis of O_3 in the presence of sea salt particles at relative humidities close to the deliquescence point led to the decay of hydrocarbons at rates indicative of chlorine atom chemistry (Behnke *et al.* 1995). Such chemistry is consistent with the observations of Keene *et al.* (1990) of halogen deficits which are greater than the excess sulphate and nitrate found in the particles. As discussed in more detail below, we have shown recently in this laboratory that the photolysis of O_3 at 254 nm in the presence of wet sea salt particles does indeed generate Cl_2 (Oum *et al.* 1998a).

Once formed, chlorine and bromine atoms can be recycled in remote regions if the reaction with O_3 is the predominant loss process. For example, Sander and Crutzen (1996) and Vogt *et al.* (1996a) have developed gas–aerosol mechanisms for marine regions in which the recycling of halogens was examined. This work suggests that, once formed, halogens can catalyse their own activation via cycling between the gas and aqueous phases, particularly in acid solutions where reactions (24) and (33) are rapid. In this chemistry, the uptake of bromine compounds from the gas phase into the particles results in the release of an additional bromine atom which originated in the particles: in the aqueous phase,

$$HOBr + Br^- + H^+ \leftrightarrow Br_2 + H_2O, \tag{24}$$

$$HOBr + Cl^- + H^+ \leftrightarrow BrCl + H_2O, \tag{33}$$

$$BrCl + Br^- \leftrightarrow Br_2Cl^-, \tag{34}$$

and

$$Br_2Cl^- \leftrightarrow Br_2 + Cl^-; \tag{35}$$

in the gas phase,

$$Br_2 + h\nu \rightarrow 2Br, \tag{36}$$

$$Br + O_3 \rightarrow BrO + O_2, \tag{22}$$

$$BrO + BrO \rightarrow 2Br + O_2, \tag{23}$$

$$BrO + HO_2 \rightarrow HOBr + O_2, \tag{25}$$

and

$$Br + HO_2 \rightarrow HBr + O_2. \tag{37}$$

The reactions of HOBr with solid NaCl and KBr have been studied recently by Mochida *et al.* (1998) using a Knudsen cell. In contrast with the aqueous phase reaction in acid solutions, the reaction of HOBr with solid NaCl is slow, with an upper limit to the reaction probability of $\gamma < 6.5 \times 10^{-3}$, but the KBr reaction may be faster ($\gamma < 0.18$). HOBr and HOCl have been proposed as oxidants for dissolved SO_2(S[IV]) in sea salt particles (Vogt *et al.* 1996a). As a result of such autocatalytic chemistry (for example Wayne *et al.* (1995)), halogen atoms can have a greater impact than implied by their initial rates of formation.

In short, a variety of laboratory, field and modelling studies suggests the importance of tropospheric halogen atom chemistry in the marine boundary layer and

marine coastal regions, in the Arctic at polar sunrise and in some unusual or episodic situations associated with certain volcanic eruptions, inland alkaline seas and certain industrial areas (Hov 1985). Understanding the chemistry on a molecular level is clearly essential for incorporating such reactions into models of the remote and polluted troposphere. We discuss in the remainder of this article some studies carried out in this laboratory directed to this question.

3. Laboratory studies of the reactions of powders of NaCl and synthetic sea salt

3.1. *Formation of unique surface nitrate species*

All the reactions of NaCl with oxides of nitrogen (reactions (27) and (29)–(31) above) generate nitrate, commonly shown as $NaNO_3$. However, the nitrate product is not bulk crystalline sodium nitrate, but rather a surface species which has some unusual physical and chemical properties. This has been observed both through infrared (IR) spectroscopy studies, as well as ultrahigh-vacuum techniques described in the article in this issue by Hemminger (1999).

Figure 1 is a schematic diagram of a diffuse reflectance infrared Fourier transform spectrometry (DRIFTS) system which is located in the sampling compartment of a commercial spectrometer. The light beam is directed on to the sample where it undergoes multiple reflection, scattering and absorption. The beam exiting the vacuum chamber which holds the sample is then directed to a cooled mercury cadmium telluride (MCT) detector. The system is normally used in a flow mode where a dilute mixture of the reactant in a carrier gas such as helium or air flows through the sample while spectra are recorded. There is a third window (shown at the top) which can be used to study the surface photochemistry using a xenon lamp (see below). Figure 2 shows a typical sequence of IR spectra as a function of reaction time for the reactions of NO_2 and HNO_3 respectively with NaCl (Vogt and Finlayson-Pitts 1994a). Bands are observed in the 1300–1500 cm^{-1} region, as well as in the regions around 1050 and 830 cm^{-1}. These correspond to the well known asymmetric stretch (ν_3), symmetric stretch (ν_1) and out-of-plane bend (ν_2) respectively of the nitrate ion. As seen in figure 2, they are formed in both the HNO_3 and the NO_2 reactions, confirming that the bands are indeed due to nitrate.

However, the band shapes and positions are not identical with those observed for a dilute mixture of $NaNO_3$ in NaCl (figure 3). For example, the strong asymmetric stretch in the 1300–1500 cm^{-1} region for a dilute mixture of $NaNO_3$ with NaCl is a broad band while that for the reaction (figure 2) initially consists of two rather sharp peaks at 1333 and 1460 cm^{-1}. As the reaction of NO_2 with NaCl continues, additional peaks grow in between these two, and it is only at larger extents of reaction that the band becomes broader and similar in shape to that of bulk crystalline $NaNO_3$.

These IR data suggest that, although nitrate is formed in these reactions as expected, it is not initially in the form of crystalline $NaNO_3$ but rather exists as a unique surface species. However, this surface species can be converted to bulk crystalline sodium nitrate by exposure to water vapour at pressures below the deliquescence point. Figure 4, for example, shows the change in the IR spectrum when a NaCl surface that had been reacted with NO_2 is subsequently exposed to water vapour and the sample is then heated and pumped. The spectrum changes from one having the two peaks characteristic of the surface species to a broad band characteristic of bulk crystalline $NaNO_3$.

This effect of water vapour on the spectrum is consistent with the formation of a mobile quasi-liquid layer upon exposure to water vapour. In this fluid film, surface

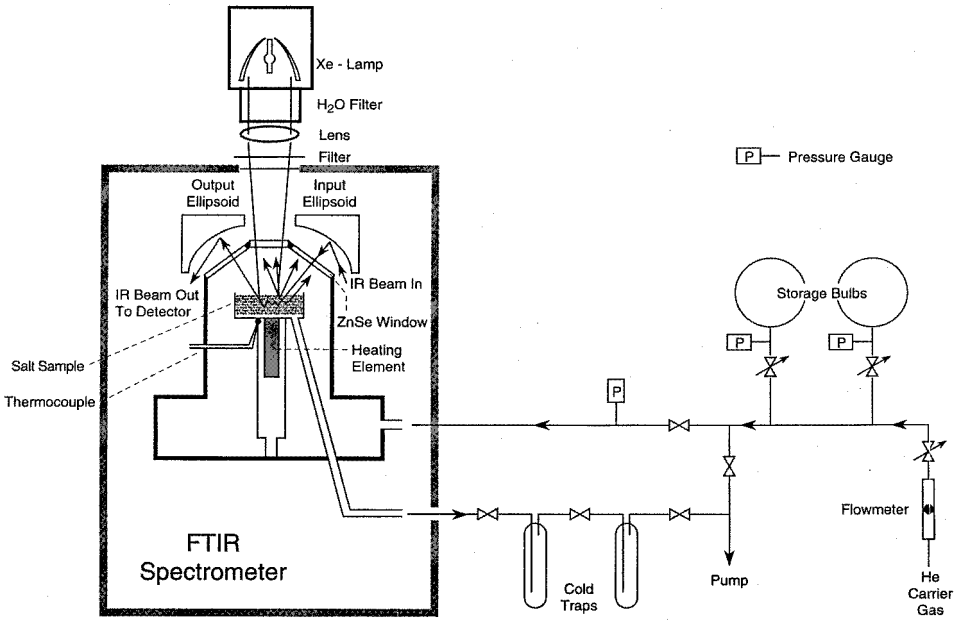

Figure 1. Schematic diagram of the DRIFTS apparatus, including the gas flow system and the photolysis port. The xenon lamp is the source of UV–visible for the photochemical studies.

nitrate, chlorine and sodium ions are mobilized. When the water is removed, selective recrystallization into small microcrystallites of $NaNO_3$ occurs, regenerating a fresh NaCl surface. As a result, when the surface is again reacted with NO_2 or HNO_3, the two sharp peaks at 1333 and 1460 cm^{-1} again are observed (figure 5), as expected for an unreacted NaCl surface.

This surface recrystallization phenomenon has been observed more directly using transmission electron microscopy (Allen *et al.* 1996, Vogt *et al.* 1996b), by atomic force microscopy (Zangmeister and Pemberton 1998) and by X-ray photoelectron spectroscopy (XPS) (Laux *et al.* 1996) as described in detail by Hemminger (1999) in this issue.

The surface nitrate has some unusual photochemical properties as well. Figure 6(*a*) shows the change in the IR spectrum when a NaCl surface which has been reacted to form surface nitrate is irradiated using a high-pressure xenon lamp. With a 1 mm Pyrex filter in place (50% transmittance at 325 nm), only small amounts of reaction occur. However, in the absence of this filter, there is increased ultraviolet (UV) in the region below 300 nm which is absorbed most strongly by NO_3^- (McCarthy *et al.* 1996). Loss of the surface nitrate then occurs readily, but the formation of nitrite, the usual photochemical product of NO_3^- (Johnson 1970), is not observed at about 1260 cm^{-1}. If the nitrate on the surface has been first exposed to water vapour and dried to convert it to microcrystallites of $NaNO_3$, bands at about 1260 cm^{-1} due to NO_2^- are formed (figure 6(*b*)). This observation thus provides additional support for the interpretation of the effect of exposure of the surface nitrate to water vapour in terms of recrystallization to form bulk $NaNO_3$.

The photochemically induced loss of nitrate without the formation of IR-absorbing products on the salt such as nitrite is somewhat puzzling. The surface nitrate may be

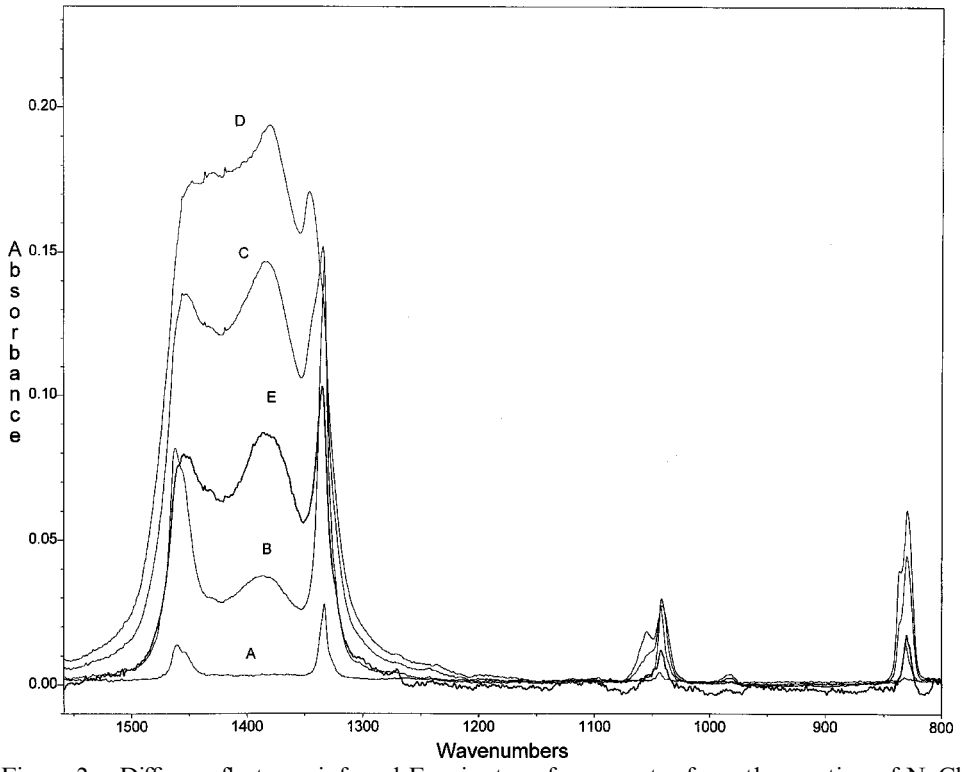

Figure 2. Diffuse reflectance infrared Fourier transform spectra from the reaction of NaCl with NO_2 (8.6×10^{14} molecules cm^{-3}) as a function of time at 298 K. Spectra A, B, C and D were recorded at reaction times of 0.5, 4.5, 23.5 and 45 min respectively. For comparison, spectrum E is from the reaction of gaseous HNO_3 (2×10^{14} molecules cm^{-3}) at 2 min reaction time.

photodissociating to $NO_2 + O^-$, rather than to $NO_2^- + O$ as occurs for bulk crystalline $NaNO_3$ (Vogt and Finlayson-Pitts 1995b). In the flow system, the NO_2 would not be observed as it is pumped off during the experiment. Given the presence of small amounts of water adsorbed on the surface (see next section), the O^- generated would be expected to react to form surface hydroxide.

In summary, IR spectroscopy has confirmed the formation of a surface nitrate species which has unique photochemistry. The formation of HNO_3 and nitrates followed by their removal, for example by deposition, has generally been considered to be the ultimate fate of oxides of nitrogen in the troposphere. However, if this photochemical decomposition of surface nitrate to NO_2 occurs to a significant extent in the troposphere, it provides a mechanism for regenerating reactive NO_2 from nitrate.

In addition, the surface recrystallization phenomenon may explain some of the field observations of halogen deficiencies in sea salt particles. For example, Mouri and Okada (1993) observed large chloride deficiencies in some smaller particles. It may be that these smaller particles were in fact microcrystallites formed by the surface reorganization, which had then sheared away from the parent sea salt particle.

In short, such studies illustrate the importance of molecular level understanding obtained from laboratory studies in interpreting field data and in developing accurate models of atmospheric reactions.

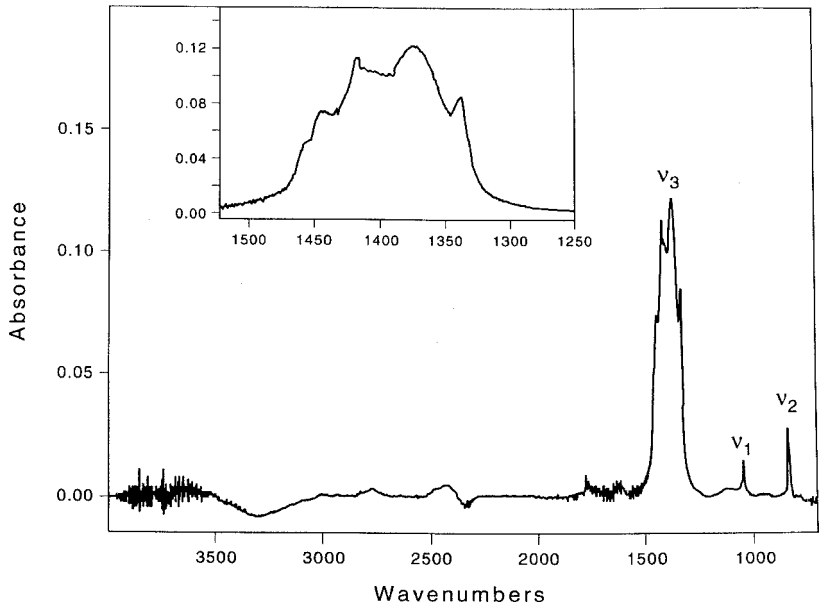

Figure 3. Diffuse reflectance infrared Fourier transform spectra of a 0.1% $NaNO_3$–NaCl mixture. Reprinted with permission from R. Vogt and B. J. Finlayson-Pitts, 1994, *J. phys. Chem.*, **98**, 3747. Copyright 1994 American Chemical Society.

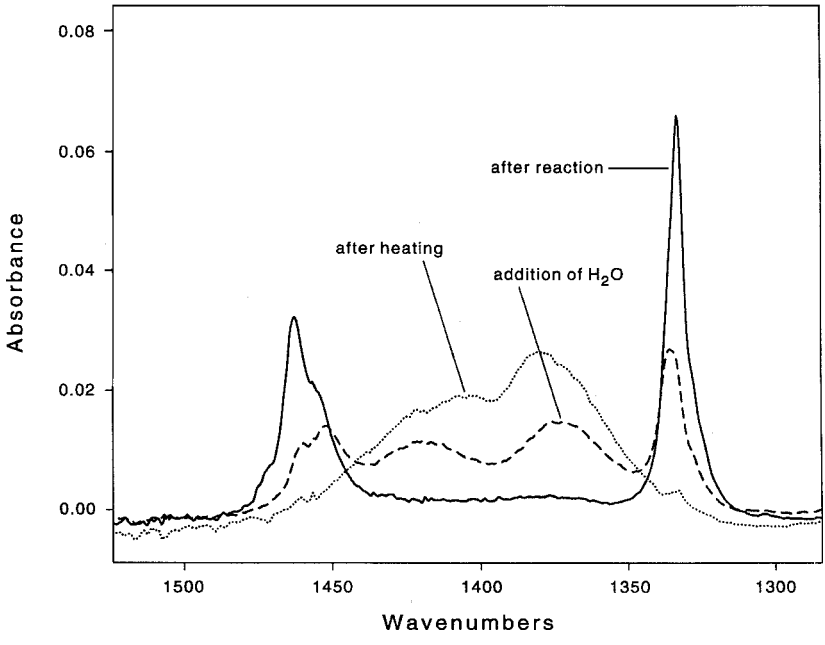

Figure 4. Diffuse reflectance infrared Fourier transform spectra of NaCl after reaction with NO_2 (4×10^{14} molecules cm^{-3}) for 16 min, then after exposure to water vapour at 17 mbar for 2 min and, finally, after heating to 413 K for 1.5 h. Note that, after exposure to gaseous water and heating, the spectrum more closely resembles that of bulk crystalline $NaNO_3$ shown in figure 3. Reprinted with permission from R. Vogt and B. J. Finlayson-Pitts, 1994, *J. phys. Chem.*, **98**, 3747. Copyright 1994 American Chemical Society.

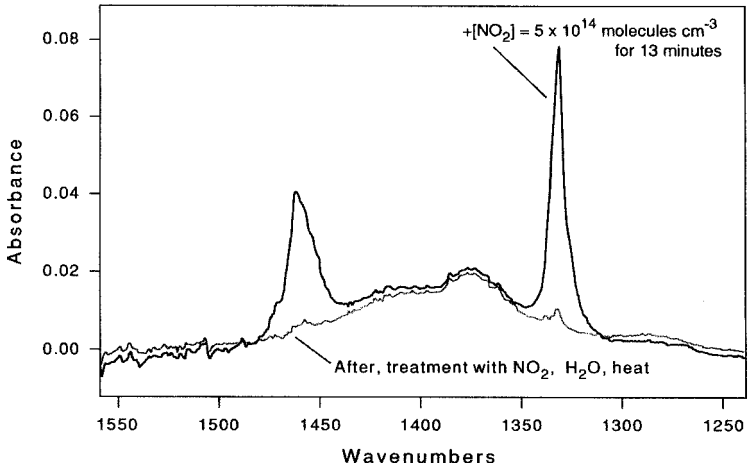

Figure 5. Diffuse reflectance infrared Fourier transform spectra after the three treatments described in figure 4, followed by reaction with NO_2 (5×10^{14} molecules cm^{-3} for 13 min). The formation of bands at 1333 and 1460 cm^{-1} is characteristic of the formation of surface nitrate on a fresh NaCl surface.

3.2. *Role of surface-adsorbed water on salt reactions*

The kinetics of reaction of HNO_3 with NaCl and synthetic sea salt have been studied by a number of groups (Fenter *et al.* 1994, 1996, Laux *et al.* 1994, Leu *et al.* 1995, Beichert and Finlayson-Pitts 1996, Davies and Cox 1998, ten Brink, 1998). Studies using ultrahigh-vacuum techniques and XPS are described in another article in this issue (Hemminger 1999). We review here briefly the results of Knudsen cell studies which not only allow determination of the reaction probability but also provide key insights into the mechanism, and in particular the controlling role of surface-adsorbed water (SAW) in the uptake and reaction of HNO_3.

Figure 7 is a schematic diagram of the Knudsen cell in this laboratory. For a detailed description of Knudsen cell techniques, see Golden *et al.* (1973), Quinlan *et al.* (1990), Fenter *et al.* (1997) and Caloz *et al.* (1997). The reactant gas enters the chamber through a series of holes located along the circumference of a circular inlet. The salt sample is held in a Teflon holder which can be heated to desorb water and other possible contaminants. The salt sample can be covered using a moveable lid mounted on a vacuum feed-through.

The experiment consists of continuous measurements of reactant gas and any gas phase products using mass spectrometry starting with the salt covered, followed by exposure of the salt to the reactant gas. A competition is set up between loss of the reactant through the aperture from the cell into the mass spectrometer, and removal by reaction with the salt. If significant uptake occurs on the salt, the fraction of the reactant gas exiting through the aperture into the mass spectrometer decreases, and the measured reactant signal intensity decreases. The reaction probability γ (defined as the fraction of collisions of gas with the salt that lead to reaction) can be obtained from the drop in the signal upon exposure of the salt to the reactant gas:

$$\gamma = \frac{A_h}{A_s}\frac{N_0 - N_r}{N_r}. \tag{38}$$

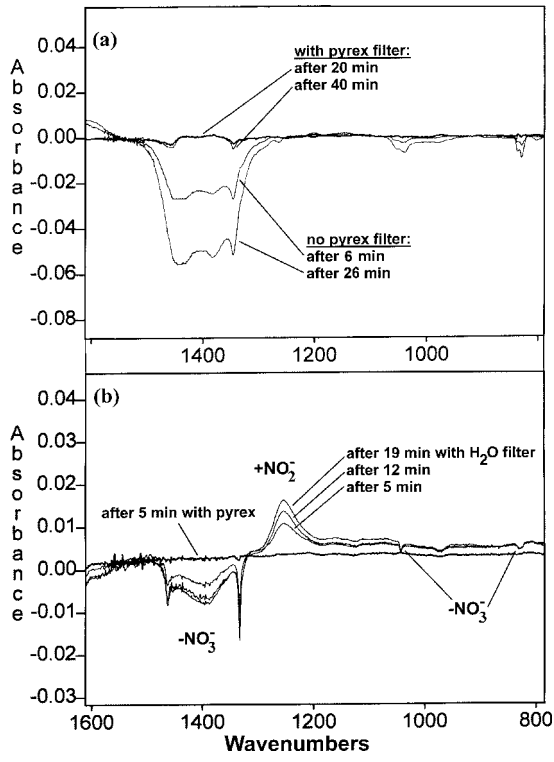

Figure 6. (*a*) Difference diffuse reflectance infrared Fourier transform spectrum obtained upon irradiation of NaCl which has been reacted with NO_2 (3×10^{15} molecules cm^{-3} for 5 min) to form surface nitrate. Changes in the spectrum upon irradiation with or without a Pyrex filter between the xenon lamp and the salt for various photolysis times are shown. (*b*) Difference diffuse reflectance infrared Fourier transform spectrum obtained upon photolysis of NaCl which has been reacted with NO_2 (1×10^{15} molecules cm^{-3} for 11 min) followed by exposure to water vapour (4×10^{17} molecules cm^{-3} for 5 min), then pumped and heated at 443 K for 5 min, followed by cooling to 298 K. This forms microcrystallites of $NaNO_3$ on the NaCl surface (see discussion in the text and in the article in this issue by Hemminger (1999)). Changes in the spectrum upon irradiation with or without a Pyrex filter between the xenon lamp and the salt for various photolysis times are shown. Note that bands due to nitrite are observed in (*b*), in contrast with the spectra in (*a*). Reprinted with permission from R. Vogt and B. J. Finlayson-Pitts, 1995, *J. phys. Chem.*, **99**, 17269. Copyright 1995, American Chemical Society.

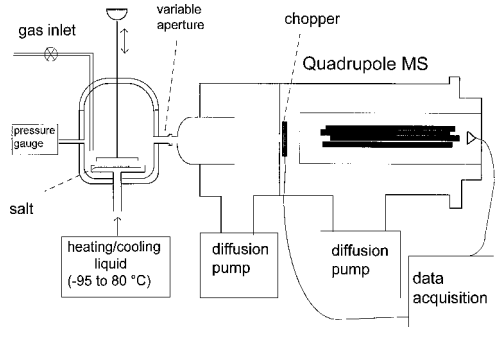

Figure 7. Schematic diagram of a Knudsen cell.

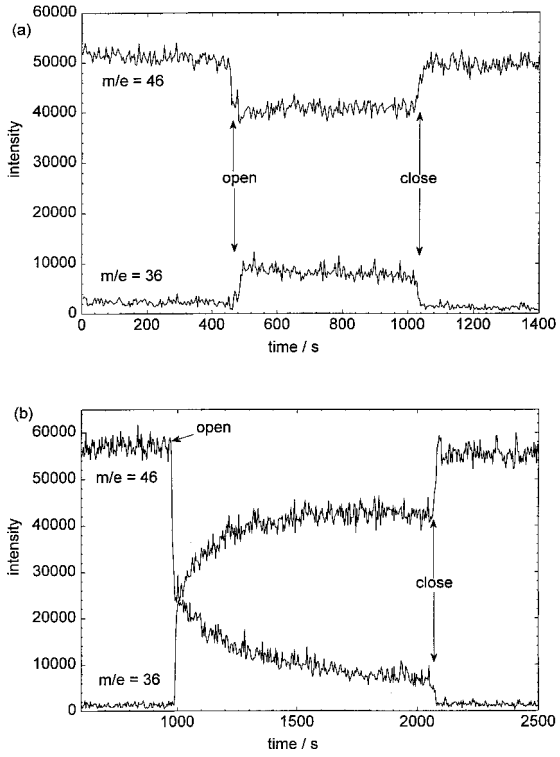

Figure 8. Uptake on NaCl powders of gaseous HNO_3 (about 0.1 m Torr) using $m/e = 46$ to follow HNO_3 at 298 K and the production of HCl ($m/e = 36$) on (*a*) particles of average diameter 500 μm heated for 6 h under vacuum and (*b*) 4 μm particles heated for 24 h under vacuum. Reprinted with permission from P. Beichert and B. J. Finlayson-Pitts, 1996, *J. chem. Phys*, **100**, 15218. Copyright 1996 American Chemical Society.

In equation (38), A_h and A_s are the areas of the aperture from the Knudsen cell into the mass spectrometer and that of the salt respectively. N_0 is the reactant mass spectrometer signal in the absence of the salt surface and N_r the signal when the lid is open to allow the gas to react with the salt. As discussed in detail by Quinlan *et al.* (1990), it is the net uptake of reactant gas which is measured in such studies. If the gas is initially taken up but then partially re-evaporates from the surface, the measured value of γ is less than the actual uptake probability.

Figure 8 shows the results of a typical experiment in which NaCl powders of two different sizes were heated and evacuated for 6–24 h followed by exposure to HNO_3 (Beichert and Finlayson-Pitts 1996). When the lid is opened to expose the salt, the HNO_3 signal at $m/e = 46$ due to HNO_3 drops as expected, and the gaseous product HCl (reaction (27)) is observed. The larger particles show a consistent uptake of HNO_3 as the lid over the salt is alternately opened and closed. The behaviour of HNO_3 in the presence of the smaller particles is similar, except that there is also a more rapid initial uptake when the salt is first exposed to HNO_3. The value of the reaction probability derived for both particle sizes at longer reaction times (i.e. ignoring the initial rapid uptake for the smallest particles) is $\gamma = (1.4 \pm 0.6) \times 10^{-2}$. Under typical experimental conditions, the time to 'saturate' the geometric surface area of the salt, that is to form a monolayer of nitrate, is calculated to be about 2 s for this reaction probability.

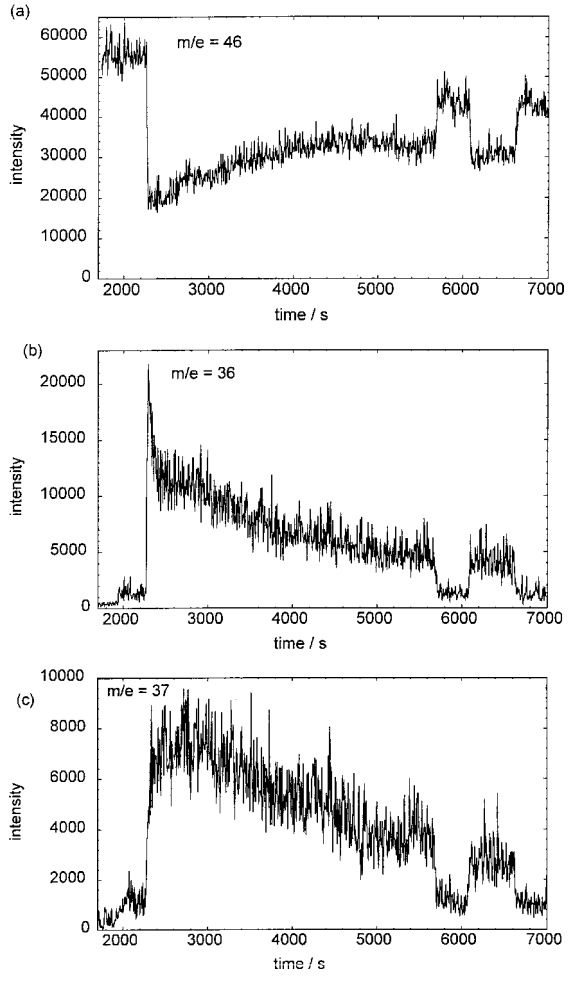

Figure 9. (*a*) Uptake of DNO_3 ($m/e = 46$), (*b*) production of HCl ($m/e = 36$) and (*c*) production of DCl ($m/e = 37$) from the reaction with NaCl powder of typical diameter 4 μm which had not been heated during pumping. Reprinted with permission from P. Beichert and B. J. Finlayson-Pitts, 1996, *J. chem. Phys*, **100**, 15218. Copyright 1996 American Chemical Society.

However, as seen in figure 8, the uptake of HNO_3 is observed for much longer periods of time and, indeed, continues on through the longest times used in these experiments (of the order of hours).

Another surprising result comes from the reaction of DNO_3 with NaCl. One would expect DCl to be the gaseous reaction product. Figure 9 shows the results of such an experiment, where DNO_3 reacted with NaCl powder which had been pumped on but not heated prior to reaction. While DCl is formed as expected, HCl is also formed and indeed, initially in larger yields than DCl.

These results are consistent with the presence of water which is sufficiently strongly adsorbed on the surface that it is not readily pumped off by the gentle heating and pumping used in these experiments. From studies of the adsorption isotherms of water on NaCl (for example Lad 1968, Dai *et al.* 1995, Dai *et al.* 1997, Peters and Ewing 1997, Shindo *et al.* 1997), it is known that there should be very little, if any, water

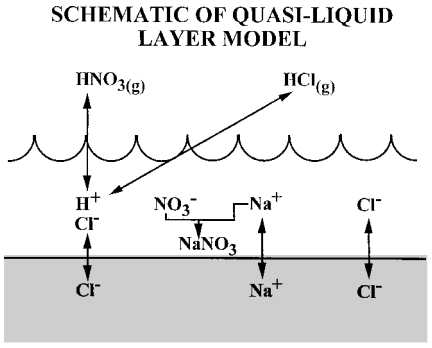

Figure 10. Schematic model of region of SAW on NaCl powders. Note that this is intended to show the unidentified site which holds water, and not the (100) surface of NaCl which does not strongly adsorb water at room temperature.

adsorbed on the (100) surface of NaCl. Hence this SAW is probably adsorbed at some (at present unidentified) crystal defects on the powder surfaces, at steps and edges or in three-dimensional voids in the crystal surface (Shindo *et al.* 1997).

Figure 10 is a schematic model of this unidentified reaction centre which is holding the SAW. It is assumed that the SAW is saturated with NaCl. The HNO_3 which is initially taken up into this solution acidifies it. When the pH becomes sufficiently low, HCl degasses from the SAW. As more HNO_3 is taken up, the solubility of $NaNO_3$ is exceeded and the excess nitrate is removed by precipitation of $NaNO_3$. NaCl continues to dissolve, HCl degasses and $NaNO_3$ precipitates out, allowing the reaction to continue for extended periods of time without evidence of 'surface saturation' that one would normally expect from the replacement of chloride by nitrate in a surface layer.

This interpretation is consistent with the well known thermodynamics of the uptake of gaseous HNO_3 and HCl into solution (for example Clegg and Brimblecombe (1985, 1986, 1988a, b, 1990), Marsh and McElroy (1985), Brimblecombe and Clegg (1988, 1990) and Tang *et al.* (1988)). It is a reasonable assumption that the SAW is saturated with NaCl, which at room temperature gives a salt concentration in the SAW of about 6.3 molal (*m*). The Henry's law constant for partioning of HCl between the gas and SAW at 298 K is $K_{HCl} = 2.04 \times 10^6$ mol^2 kg^{-2} atm^{-1} $= m_{H^+} m_{Cl^-} \gamma^2 \pm / P_{HCl}$ (Brimblecombe and Clegg 1988). The activity coefficients $\gamma^2 \pm$ can be calculated as described by Brimblecombe and Clegg (1988) and the partial pressure of HCl in the Knudsen cell is known from the mass spectrometry (MS) signals calibrated using an authentic sample of HCl. Hence the molality of H^+ and its activity in the SAW can be calculated, giving a pH of about 1.7 at equilibrium.

Similarly, the equilibrium between the gas-phase reactant HNO_3 and its concentration in the SAW can be calculated from the known Henry's law coefficient $K_{HNO_3} = 2.66 \times 10^6$ mol^2 kg^{-2} atm^{-1} $= m_{H^+} m_{NO_3} \gamma^2_{\pm} / P_{HNO_3}$ (for example Brimblecombe and Clegg (1988), Tang *et al.* (1988) and Clegg and Brimblecombe (1990)). The gas-phase HNO_3 pressure in the cell is measured and the molality of H^+ and the activity coefficients calculated as described above. The concentration of nitrate in the SAW in equilibrium with the gas-phase HNO_3 can then be calculated, which under our typical experimental conditions is about 22 *m*. This is approximately equal to the concentration of nitrate expected based on the solubility of $NaNO_3$ and the saturation concentration of Na^+ of 6.3 *m*.

In short, the continuous uptake of HNO_3 and production of HCl are consistent with uptake of HNO_3 into a saturated solution on the salt surface, acidification of this SAW and subsequent degassing of HCl. In our apparatus, the time to acidify the SAW and hence the delay time in HCl production is too short to be observed. However, Fenter *et al.* (1994) did observe an induction period for HCl production using lower concentrations of HNO_3, consistent with our interpretation. In addition, this group has also recently reported evidence for SAW on their salt crystals (Seisel *et al.* 1997). Davies and Cox (1998) reported that the uptake coefficient for HNO_3 showed a similar dependence on water vapour pressure as the isotherm for adsorption of water on NaCl powders, suggesting that it is controlled by the volume of adsorbed water. They also reported that the uptake coefficient decreases with increasing concentrations of gaseous HNO_3 and interpret this in terms of a Langmuir type of dissociative adsorption of HNO_3.

In summary, although the (100) face of single-crystal NaCl does not readily take up water at room temperature and low water vapour pressures, NaCl powders have some strongly bound water at some as yet unidentified surface sites. This SAW behaves like a solution in its behaviour towards the uptake and reaction of HNO_3. Studies are currently under way in this laboratory to assess the role of this SAW in other reactions of NaCl, such as those with N_2O_5 and $ClONO_2$. The accompanying article by Hemminger (1999) discusses the results of XPS studies which show the presence of oxygen in some form on the surface of NaCl powders, but not on the (100) face of single crystal NaCl, at room temperature.

The realization that there was strongly adsorbed water on the salt surface which controls the uptake and reaction of gaseous HNO_3 is another example of the importance of understanding the kinetics and mechanisms on a molecular level. The reaction probability for HNO_3 with NaCl powders derived from studies in this (Beichert and Finlayson-Pitts 1996) and other laboratories (Fenter *et al.* 1994, 1996, Leu *et al.* 1995) are all in excellent agreement at about $(1–2) \times 10^{-2}$. As discussed by Hemminger (1999), the reaction probability on the (100) face of single-crystal NaCl in the absence of water is much smaller, 4×10^{-4} (Laux *et al.* 1994). However, Davies and Cox (1998) report that the reaction probability decreases with increasing HNO_3 and increases with increasing water vapour; potential mechanisms to explain this are discussed by Hemminger (1999). Recognizing that water will of course always be on salt surfaces in the troposphere allows one to select the appropriate value for use in tropospheric models. However, the single-crystal work is central to understanding the significance of SAW and, in particular, its controlling role in the reaction.

3.3. *Reactions of synthetic sea salt: is NaCl an appropriate surrogate for sea salt?*

Although NaCl has been used in this and other laboratories as a model for sea salt, real sea salt particles contain a variety of other components, including transition metals and crystalline hydrates such as $MgCl_2 \cdot 6H_2O$. Figure 11 shows the spectra obtained by DRIFTS from the reaction of synthetic sea salt (Instant Ocean®) with NO_2. Bands in the regions expected for nitrate are again observed, but they are not identical with those for the NaCl reaction. Figure 11 also shows the IR spectrum for the reaction of NO_2 with $MgCl_2 \cdot 6H_2O$, a major component of sea salt, under similar conditions. The nitrate bands formed in the synthetic sea salt reaction are quite similar to those from the reaction of $MgCl_2 \cdot 6H_2O$, suggesting that crystalline hydrates play a major role in the chemistry of sea salt particles (Langer *et al.* 1997). It is interesting

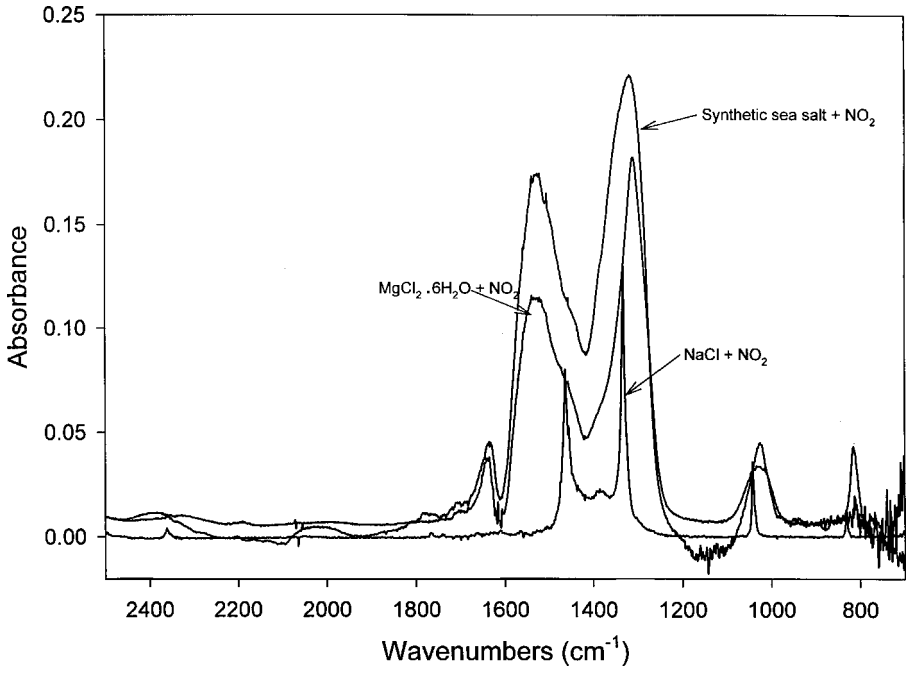

Figure 11. Diffuse reflectance infrared Fourier transform spectra from the reaction of NO_2 with NaCl (6.6×10^{14} molecules cm^{-3} in air for 3.5 min), with synthetic sea salt (2.4×10^{15} molecules cm^{-3} for 40 min in air) and with $MgCl_2 \cdot 6H_2O$ (8.6×10^{14} molecules cm^{-3} in air for 45 min).

that, for the reaction of both $MgCl_2 \cdot 6H_2O$ and synthetic sea salt, a band at 1635 cm^{-1} forms during the reaction. This is assigned to SAW which has several possible sources. The waters of hydration bound in the crystal structure of hydrates such as $MgCl_2 \cdot 6H_2O$ may be released if the crystal structure is disrupted by reaction (Langer *et al.* 1997). Another potential source is the release of water trapped between salt crystals in the sample-handling process.

Knudsen cell studies of the reaction of HNO_3 with synthetic sea salt (De Haan and Finlayson-Pitts 1997) show qualitatively similar behaviour to that of the NaCl reaction. However, the role of SAW is greatly amplified, presumably owing to the presence of highly hygroscopic components such as $MgCl_2 \cdot 6H_2O$. In addition, because of these hygroscopic components, the salt particles tend to clump together and there may be some water trapped between crystals which is released during the reaction. Indeed, there is sufficient SAW on synthetic sea salt that the exchange with gas phase D_2O can be readily measured (De Haan and Finlayson-Pitts 1997). As a result, even under conditions of lengthy gentle heating and pumping, the minimum measured value of the reaction probability is still a factor of about six greater than for similarly treated NaCl. The measured values of the reaction probability for HNO_3 with synthetic sea salt ranged from about 0.07 to 0.75, depending on the pre-treatment of the salt, particularly heating and pumping to remove adsorbed water. Thus, under conditions relevant to the atmosphere, the uptake is more than an order of magnitude greater than for NaCl (De Haan and Finlayson-Pitts 1997).

In short, while the reactions of NaCl appear to mimic qualitatively those of sea salt, there are some important quantitative differences related to increased amounts of

SAW in the case of sea salt. The key role of the crystalline hydrates in the kinetics and mechanism of the reactions again illustrates the importance of understanding these processes on a molecular level.

4. Aerosol chamber studies

The studies described above and in the article by Hemminger (1999) all involve reactions of solids, in either powder or single-crystal form. As we have seen, water on the surface of powders can play a significant role in the chemistry. As a result, studying the chemistry of salt aerosol over a range of relative humidities (RHs) both below and above their deliquescence point where the particles are concentrated aqueous solutions is important. In the latter case, the concentration of dissolved salt in such particles varies with the relative humidity (for example Tang *et al.* (1977, 1978, 1997) and Tang and Munkelwitz (1984, 1993)). At higher RHs, there is more water uptake and hence the solutions are more dilute. For example, for NaCl at 97% RH at room temperature, the liquid particles have a solute concentration of 5 wt% (0.9 M), compared with 26 wt% (6.1 M) at the deliquescence point of 75% RH. Sea salt particles show similar behaviour (Tang *et al.* 1997).

In short, studies in which the RH, particle composition and size and gas composition can be varied have the potential to provide insights into how the mechanism changes as one moves from a 'dry' solid such as those discussed earlier, to aqueous solutions.

We have recently designed and constructed an aerosol chamber to carry out studies of the uptake and reaction of gases with both solid and liquid particles over a range of RHs. We describe here its features and characterization, including the results of some studies which illustrate differences in the chemistry of aqueous particles compared with solids (even those holding adsorbed water).

This chamber was constructed to allow the study of the interactions of gases with liquid and solid particles in real time and under conditions which mimic those of the atmosphere. Photochemical studies can also be performed. Particle number densities and size distributions can be varied, thereby controlling total particle surface area and volume. Control of RH and temperature in the chamber allows either liquid or solid salt particles to be studied. Finally, the chamber is interfaced to optical detection systems which directly measure the spectroscopic properties of relevant gas-phase and condensed-phase species in real time. In addition, an atmospheric pressure ionization mass spectrometer is interfaced to the chamber for the measurement of gas-phase reactants and products which cannot be measured using UV–visible or IR spectroscopy.

4.1. *Design considerations*

A modular design, with parts that could be routinely switched, reconfigured or even remachined as needed without requiring the chamber itself to be moved or substantially disassembled, was used to optimize the long-term usefulness of the chamber. Specifically, a design where even the pumping and sampling ports could be readily moved to accommodate both static and flowing experiments was desired. In addition, these parts were to be moveable without disturbing optical alignments inside the chamber. These alignments were to remain stable with respect to changing temperatures (248–348 K), water vapour concentrations (about 10^{15}–10^{17} molecules cm^{-3}) and pressures (10^{-4}–1 atm) and must also be easily accessible for adjustment and cleaning. An illumination system for UV and visible photolysis studies which evenly illuminates the chamber volume was also desired.

Chamber materials were to be vacuum compatible, unreactive towards the gaseous reactants and products in each experiment, and not electrostatically attractive towards charged particles. However, since no material (or coating) meets these criteria perfectly, the chamber was made as large as possible to minimize the surface-to-volume ratio, keeping within limits imposed by reactant fill times and construction and operation expenses.

Finally, the chamber was to be interfaced directly to analytical instrumentation which is able to follow the chemical composition of gases and particles *in real time* over a range of concentrations approaching ambient atmospheric concentrations.

4.2. *Chamber design*

The chamber has two main parts: a solid aluminium optical bench (the 'baseplate') and a stainless steel chamber frame which sets on top of it. The frame seals to the baseplate via an ethylene propylene di-monomer (EPDM) O-ring in a groove machined into the baseplate and is held in place primarily by its own weight. A series of finger-tightened bolts secure the frame to the baseplate to prevent catastrophic movement, while allowing interplay between the two parts for thermal expansion (design range, ambient $\pm 100^{\circ}$C). A schematic diagram is shown in figure 12. The solid Al6016 aluminium alloy baseplate (241 cm $\times$ 53 cm $\times$ 5 cm) prevents flexing (and misalignment of optics) during pump-down. The steel frame (48 cm $\times$ 48 cm $\times$ 221 cm, outer measurements) is machined from six plates of ST316 stainless steel 2.5 cm thick which are attached to each other with 3 mm overlap by structural spot welds on the outside of corner joints and continuous vacuum welds on the inside of corner joints.

No vacuum-incompatible materials (such as plastics) were utilized in any part of the chamber interior or on the optics systems inside. All machined parts were cleaned with pentane (Fisher Scientific; 99.8%) to remove residual machining fluids. Steel parts were then further cleaned with trichloroethylene (Fisher Scientific; 99.9%).

The chamber surface area is 4.7×10^4 cm^2 and the volume is 5.6×10^5 cm^3, giving a surface-to-volume ratio of 0.08 cm^{-1}. For a typical polydisperse aerosol (see below), the particle surface area is about 1% of the total chamber surface area.

The steel frame holds 17 interchangeable aluminium panels (41 cm $\times$ 41 cm), which seal to the frame with EPDM O-ring seals. The panels are machined from Al6016 aluminium alloy plates 2.5 cm or 3.8 cm thick. Several different types of panel were constructed. A pumping panel was interfaced to a Klein-flange adapter of 5.1 cm inside diameter with an EPDM O-ring seal for further attachments of a high-vacuum valve and pumping line. Several panels have attached fittings for gas and aerosol addition and sampling, optical ports and the insertion of temperature and humidity probes. All fittings are attached to panels by either EPDM O-ring seals or Teflon-taped stainless steel NPT threads.

Six window panels were constructed such that each panel could hold four interchangeable square Pyrex or quartz plates. These window panels are typically placed along the top and one end of the chamber as shown in figure 12. Both synthetic fused silica quartz (Heraeus–Amersil SFS-010) and borosilicate glass (Newport Industrial Glass) plates are 16.5 cm square and 1.3 cm thick and either set can be seated on 5 mm cross-section diameter EPDM O-rings. The O-ring seal is designed so that the window will never fully compress the O-ring and come into contact with the aluminium alloy panel, even at full vacuum.

An aluminium alloy frame system supports a row of photolysis lamps above the chamber. The height, position and number of lamps can be adjusted. The lamps are

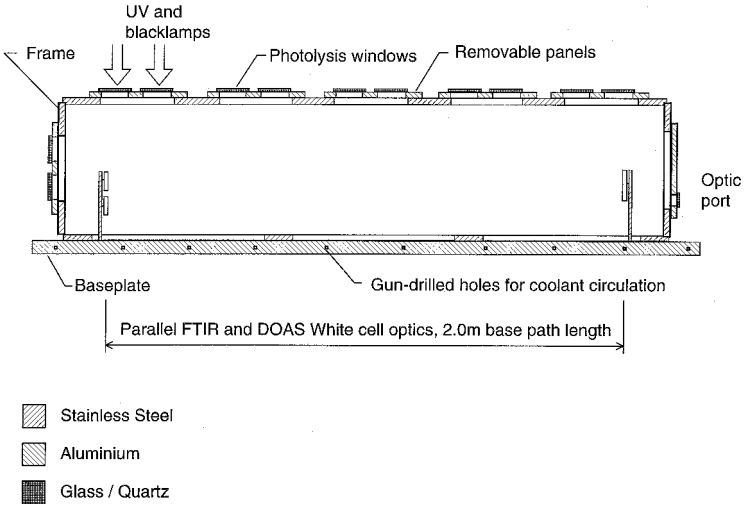

Figure 12. A schematic cut-away view of the chamber. The mirrors for the parallel long path White cell systems for FTIR spectrometry and DOAS are shown inside the chamber. Each side of the chamber is covered with five removable panels. Window panels are installed on the top and the left side.

fitted with interchangeable low-pressure mercury (UVP XX-15S; 1.68 mW cm^{-2} at 30 cm distance) or black-lamp bulbs (UVP XX-15BLB; 0.73 mW cm^{-2} at 30 cm distance).

The pumping system consists of a mechanical rotary roughing pump (Edwards model 1397; 17.7 cfm) and a series of steel sorption pumps (Huntington Mechanical Laboratories Inc. EV-150-SF) attached to a switching manifold. The mechanical pump evacuates the chamber from 1 atm down to pressures of 2 Torr in approximately 10 min, at which point pumping is switched over to a cooled sorption pump. The switch is made well above the mechanical pumping limit to avoid backstreaming of oil vapours into the chamber. For the same reason (and to protect the pumps from corrosive gases), a liquid-nitrogen trap is placed between chamber and pumps. The chamber pressure is routinely monitored by a 1000 Torr diaphragm gauge (Leybold CMH1000) while pressure in the pumping manifold is measured with a Pirani gauge with a corrosion-resistant platinum sensor element (Leybold TR216). The chamber is filled by tank ultrahigh purity air or nitrogen, supplied by Scott–Marrin (Riverside, California).

Temperature control is achieved by circulating fluid through gun-drilled holes in the aluminium alloy baseplate and many of the attached aluminium alloy panels. Large pressure differentials are avoided by using manifolds to circulate fluid in parallel paths, rather than in series. Fluid circulation and temperature regulation are provided by a unit with a 3 kW heater, 12 kW cooling power at 0°C, and 76 l min^{-1} fluid pumping capacity (FTS, Stoneridge, New York; manufacturer specified temperature range is -38 to 75°C). This fluid-circulating system utilizes an external temperature probe to the monitor and control chamber temperatures.

Humidity is added to the chamber by sending part of the fill gas through large glass-frit water bubblers containing Nanopure water (Barnstead; $\rho > 18$ MΩ). By varying the relative flow rates of dry and completely humidified gas streams, the RH of a gas fill could be set to within about 5% RH of a target value. The RH (resolution,

$\pm$0.1%) and temperature (resolution, $\pm$0.1°C) are monitored by three sensor probes (Vaisala HMP234) which extend through chamber panels and sample the central volume of the chamber.

All exposed surfaces in the chamber, with the exception of optical surfaces and the ends of the temperature and humidity probes, were made chemically inert by coating with halocarbon wax (Halocarbon Products Corporation series 1500). Coating was performed by heating each part of the chamber to the point where the wax softens and spreading wax across all exposed surfaces. The reassembled chamber was then heated to the wax-softening point and pumped for extended periods. This solvent-free coating technique was used to ensure that solvent outgassing from the wax coating would be insignificant. However, certain small parts (chiefly optics stands and holders) were coated by dipping them into hot solutions of methylene chloride saturated with halocarbon wax, followed by air drying. Approximately 100 g of halocarbon wax was required to coat all chamber surfaces.

Since halocarbon wax is not conductive, static charges may exist at the wax surface and cause particle losses by electrostatic attraction. Although these losses are minimized by producing a Boltzmann charge distribution on the particles (see section 4.3.5), electrostatic attraction to the walls is still expected to be the dominant loss mechanism for particles in the size range 0.1–1.0 μm (McMurry and Rader, 1985).

Ozone was produced by flowing ultrahigh-pressure oxygen through a small UV-photolysis-based ozonizer (Sander model 25) with an adjustable output. The ozone production rates were calibrated using a commercial ozone monitor (Dasibi Environmental Co. model AH1001, Glendale, California).

4.3. *Analytical systems*

4.3.1. *Overview*

The analytical systems interfaced to the aerosol chamber were selected for their sensitivity, their ruggedness and their ability to detect complementary species. *In-situ* long-path spectroscopy was performed with both a Fourier transform infrared (FTIR) spectrometer and a differential optical absorption spectrometer operating at UV–visible wavelengths. These instruments can detect, identify and quantify many of the gas-phase and some condensed-phase species, such as nitrate and sulphate, of interest in these studies. Since absolute absorbance values at a particular wavelength are subject to interference from aerosol scattering and extinction, differential optical absorption techniques are particularly useful. An atmospheric pressure ionization tandem mass spectrometer allows the detection and positive identification of many other compounds which lack suitable UV or IR absorption spectra. In addition, a scanning mobility particle sizing and counting system is used to monitor particle size distributions. A schematic diagram of the coupled instrumentation is shown in figure 13.

4.3.2. *Fourier transform infrared spectrometry*

The FTIR spectrometer uses an air-cooled mid-IR source and has a maximum resolution of 0.15 cm^{-1}. An automated moveable mirror sends the IR beam to external gold-coated optics which focus the beam through a zinc selenide window (1° wedge) into the first set of White (1942) cell optics located inside the aerosol chamber. Zinc selenide is used because it is not sensitive to water vapour, is relatively unreactive and transmits a reasonably large wavelength range.

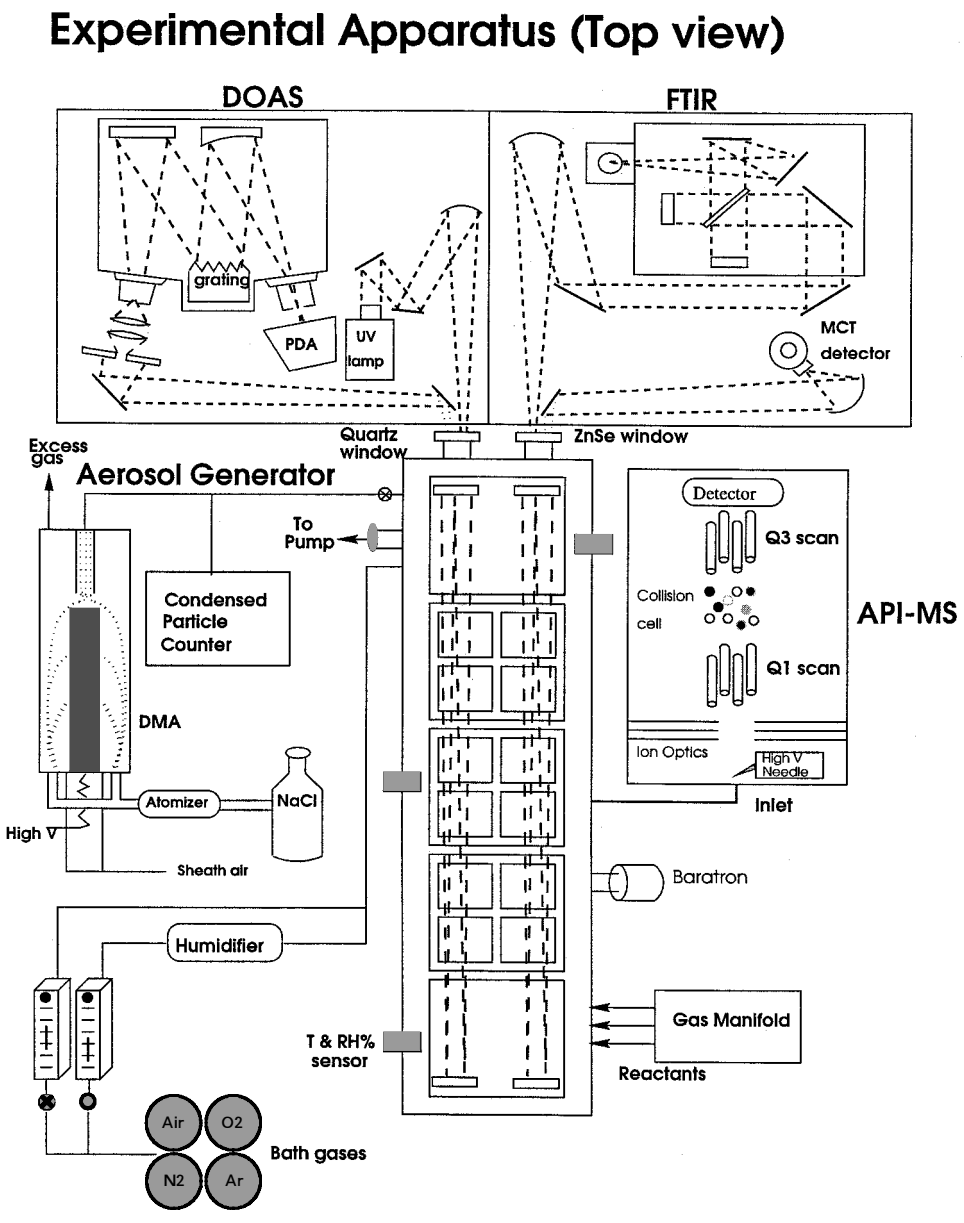

Figure 13. Experimental apparatus (top view): PDA, photodiode array; DMA, differential mobility analyser. The broken lines inside the chamber indicate the light path of the UV lamp (for DOAS) and IR source (for FTIR spectrometry).

The base path lengths of the dual White cells are 2.0 m. By changing the number of passes through the cell, the total IR optical path length is easily varied between 12 and 52 m. Path lengths longer than 52 m could be obtained using a smaller IR beam spot on the mirror above the system focal point. White cell IR optic sets are coated with either protected silver or gold. The reflectivity of the mirrors is measured by changing the number of reflections in the White cell with the chamber open and is greater than 99% for the silver IR mirrors (over the range 5000–500 cm^{-1}, measured

only in regions free of water and CO_2 bands). Borosilicate glass flat mirror blanks (Edmund Scientific, Barrington, New Jersey) and non-flat mirrors (machined by J. Brunash, Carlsbad, California) were coated by QSP Optical Technology (Santa Ana, California).

The FTIR spectrometer has a deuterated triglyceride sulphide detector on the internal beam path (through the instrument's sample compartment) and an external MCT detector. A gold-coated off-axis paraboloid mirror focuses the infrared beam from the White cell onto the sensing element of the MCT detector.

Detection limits (calculated as ten times the rms noise) for the compounds of interest using the FTIR method at a path length of 52 m range from 75 ppb for $ClNO_2$ to 2 ppm for NO.

4.3.3. *Differential optical absorption spectrometry*

A high-pressure xenon arc lamp serves as a light source for UV–visible spectroscopy. Condenser lenses focus the brightest part of the lamp arc through a 25 μm pinhole and then collimate the beam. A set of 'protected-aluminium'-coated mirrors focus the beam through a quartz window (1° wedge) into the second parallel set of White cell optics in the chamber.

The UV–visible cell can be operated either in the usual White cell multipass design (White 1942) or in a revised mirror design (White 1976) which uses small mirror pairs to fold the light path more efficiently, readily achieving optical path lengths as long as 136 m. The path length is currently limited by the number of focal spots that can be fit on the field mirror in the White cell focal plane. UV–visible optics are coated with either 'protected aluminium' or a dielectric coating (QSP Optical Technologies). Reflectivity of protected aluminium mirrors reaches a maximum of 91% at 320 nm; thus, the low transmittance of the White cell after multiple reflections is a second limit on optical path lengths using this type of mirror coating. The dielectric-coated mirrors are specified to have a reflectivity greater than 99.5% over a relatively narrow wavelength range (300–340 nm) and can be used for long-path measurements within this range.

A Jobin–Yvon–Spex Czerny–Turner type of spectrograph (model 460MST24) fitted with a holographic grating (1200 g mm^{-1} blazed at 330 nm) and a 1024 element photodiode array (Princeton Instruments PDA-1024 ST121) serves as the ultraviolet–visible detection system. A set of lenses focuses the ultraviolet beam as it emerges from the chamber White cell on to the entrance slit of the spectrometer. The dispersion of the spectrometer is 0.04 nm per pixel, giving a spectral interval of approximately 40 nm, which is selected by rotating the grating. The resolution of the spectrograph (0.24 nm) is determined by the entrance slit width of 150 μm.

The data acquisition and spectral analysis software (Gomer *et al.* 1995) uses DOAS techniques developed for atmospheric measurements (reviewed by Platt (1994)) to identify and quantify species with relatively narrow absorption bands (smaller than about 5 nm). This allows one to use the characteristic bands to distinguish the absorbing gas from the broad-band background scattering by gases and particles. The algorithms utilize a combination of linear and nonlinear least-squares fitting routines to scale multiple reference spectra to experimental spectra and thus minimize residual absorbance structures. Since differential optical absorption spectra can shift by a pixel in spectral position over time owing to thermal drift of the spectrograph, nonlinear fitting routines can improve accuracy by making small adjustments to the wavelength scales ('shift' and 'squeeze') during the fitting procedure.

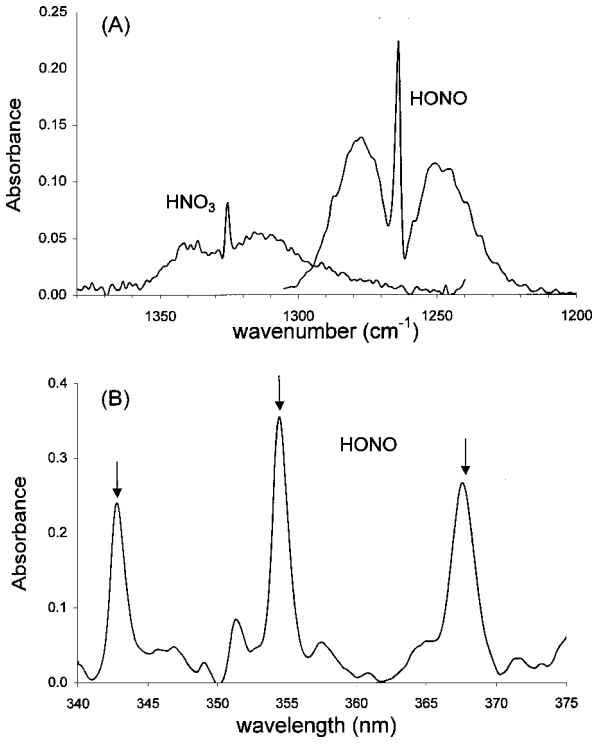

Figure 14. Typical sample spectra: (*a*) FTIR spectrum of 1 ppm HNO_3 and 6 ppm HONO, where the path length was 52 m and the resolution was 1 cm^{-1}; (*b*) differential optical absorption spectrum of HONO in the 340–375 nm region where the arrows indicate the HONO peaks in this region. HONO was generated from the ClNO+ H_2O reaction and both FTIR and differential optical absorption spectra were taken from the same experiment within five minutes of each other. Some of the small peaks in (*b*) are from NO_2.

Figure 14 shows some typical FTIR and differential optical absorption spectra of HONO acquired simultaneously, as well as HNO_3 by FTIR spectrometry. The HONO was generated from the reaction of ClNO with water vapour. The combination of both DOAS and FTIR spectrometry is particularly powerful in that all species, including the reactant ClNO (not shown), can be measured accurately in real time with high sensitivity. In the particular case shown in figure 14, the HONO concentration was sufficiently large that it could be detected by both FTIR spectrometry and DOAS. However, for many systems and reaction conditions of interest, HONO is at sufficiently small concentrations that it can only be detected by DOAS.

4.3.4. *Atmospheric pressure ionization tandem mass spectrometry*

MS analysis of the chamber contents is performed by connecting a chamber port to the ionization region of the atmospheric pressure ionization mass spectrometer (Perkin–Elmer Sciex model API-300) via a short length of glass tubing. Ionization at atmospheric pressure occurs at the tip of a corona discharge electrode. In the positive-ion mode, ionization typically occurs by proton transfer from a hydronium ion to give an [M+ 1] peak. In the negative ion mode, parent ions ([M] peak) are commonly generated by electron transfer from O_2^- and its clusters with water and O_2. The efficiency of these transfer reactions vary for each compound, necessitating a

calibration for each compound which is to be detected quantitatively. Ions and neutrals from the corona region are swept into the first quadrupole region through a series of differential pumping stages. Ions exiting the first quadrupole can be collisionally dissociated in a second quadrupole region, and the fragments analysed by a third scanning quadrupole (Spicer 1994). These dual selection processes allow parent and fragment ions for relatively simple compounds to be unequivocally identified.

4.3.5. *Aerosol equipment*

The aerosol is generated and sized by commercial instrumentation (TSI, St Paul, Minnesota). The constant output atomizer (model 3076) produces a polydisperse aerosol at a number density of 10^6–10^7 particles cm^{-3} and a flow rate of 3.0 l min^{-1}. The time to add sufficient aerosol to the 560 l chamber to give a particle concentration of about 10^5 cm^{-3} is approximately 10 min. For a 1.0% w/w synthetic sea salt solution, the resultant aerosol distribution is centred around 0.1–0.2 μm diameter after drying the air stream. The size distribution is log-normal and depends on the salt concentration in the solution being atomized. The dried aerosol is sent through charge neutralizers (TSI model 3077 or NRD Inc. model 2U500, Grand Island, New York), which give the collection of particles a Boltzmann equilibrium distribution of charge centred around zero, such that 91% of particles (at $D_p = 0.1$ μm) have a charge of ± 1 or less (Hinds 1982, Wiedensohler 1988). Charge neutralization increases the average lifetime of particles in the chamber by reducing electrostatic attraction to the walls.

The aerosol number density and size distribution is monitored by a scanning mobility particle sizing (SMPS) system (TSI), which sizes particles using a scanning electrostatic classifier (model 3071) and counts them using butanol condensation and a laser scattering counter (model 3025). This integrated system operates in both overpressure and underpressure modes, allowing the direct characterization of either the atomizer output or the aerosol in the chamber within the size range 0.003–1.0 μm. Monodisperse aerosol can also be generated by setting the particle electrostatic classifier at one voltage and diverting the output directly into the chamber.

4.4. *Chamber characterization*

After the optics were installed, the linearity of absorbance against path length was verified for the FTIR and DOAS systems. Initial tests were performed using protected-silver-coated mirrors on the IR White cell and protected-aluminium-coated mirrors on the UV–visible White cell. These coatings also performed well during chamber chemical reactivity tests (see below).

The reactivity of the wax-coated chamber walls towards many tropospherically relevant gases was tested before the chamber was exposed to any aerosol particles. Single compounds were added to the chamber in ultrahigh-purity air at concentrations of a few parts per million, under various humidity conditions. First-order wall loss rate constants were calculated using time-dependent FTIR or DOAS measurements of the compound added to the chamber. These data, summarized in table 2, provide a 'clean chamber' baseline for comparison against future measurements of wall reaction rates, which may be altered over time by the deposition of reactive particles. It can be seen that water vapour significantly enhances the wall loss rates of most of these compounds. Reactions on the chamber walls produced only the expected products for each reaction.

After the behaviour of gases was characterized in the clean coated chamber, the wall loss rates of aerosol particles were measured with the SMPS system for NaCl,

Table 2. Wall loss rates for some gases of interest in the aerosol chamber in air at 1 atm.

Gas	RH (%)	k_w (s^{-1}) ($\pm 2\sigma$)
O_3	0.3	$(6.2 \pm 0.1) \times 10^{-6}$
	50	$(8.4 \pm 0.2) \times 10^{-6}$
NO_2	0.2	$(4.3 \pm 0.1) \times 10^{-6}$
	54	$(1.2 \pm 0.3) \times 10^{-5}$
ClNO	0.2	$(5.9 \pm 0.1) \times 10^{-6}$
	51	$(4.2 \pm 0.1) \times 10^{-4}$
$ClNO_2$	0.1	$(5.9 \pm 0.2) \times 10^{-6}$
	55	$(2.5 \pm 0.3) \times 10^{-4}$
$ClONO_2$	0.2	$(2.1 \pm 0.6) \times 10^{-4}$
	61	$(1.7 \pm 0.2) \times 10^{-3}$
HNO_3	0.1	$(4.0 \pm 0.03) \times 10^{-5}$
	61	$(1.4 \pm 0.03) \times 10^{-3}$
N_2O_5	0.8	$(9.2 \pm 0.1) \times 10^{-5}$
HCl	0.1	$(5.3 \pm 0.02) \times 10^{-6}$
	56	$(9.8 \pm 0.3) \times 10^{-4}$
NO	0.7	$(4.2 \pm 0.35) \times 10^{-7}$
	53	$(1.5 \pm 2.5) \times 10^{-6}$

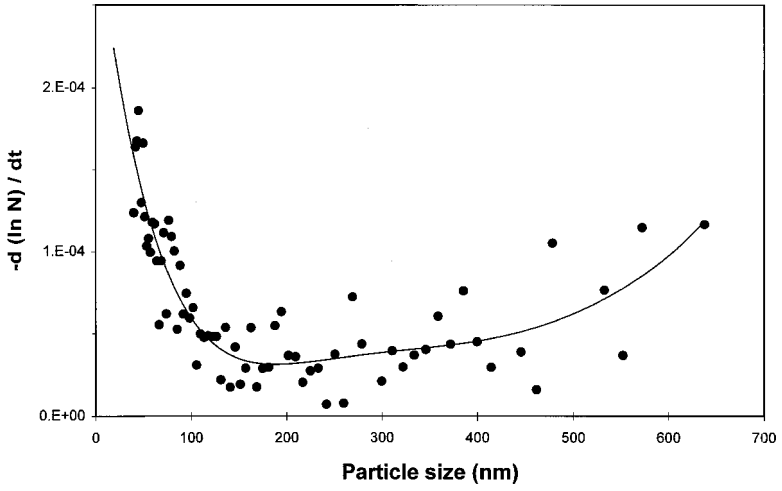

Figure 15. Size-dependent particle loss rates for sea salt particles in the chamber measured with the SMPS system. Loss rates were taken from the slopes of temporal depletion of the particle numbers at 0, 1.3, 2.8 and 3.8 h respectively. The solid curve is provided as a guide to the eye only.

synthetic sea salt and $NaNO_3$ aerosols. Typical aerosol particle concentrations used in the chamber are in the range 10^4–10^5 cm^{-3} with a geometric number mean diameter of 0.15 μm and a geometric standard deviation of 1.9 for polydisperse aerosols. Typical surface and volume concentrations are 10^{10}–10^{11} nm^2 cm^{-3} and 10^{12}–10^{13} nm^3 cm^{-3} of air respectively. However, for monodisperse aerosols, the total particle number density is much lower (about 10^3 cm^{-3}) because of the selection of a very narrow size range of particles.

Size-dependent particle loss rates for sea salt particles are shown in figure 15. The higher loss rates of particle sizes less than 50 nm are due to Brownian and turbulent

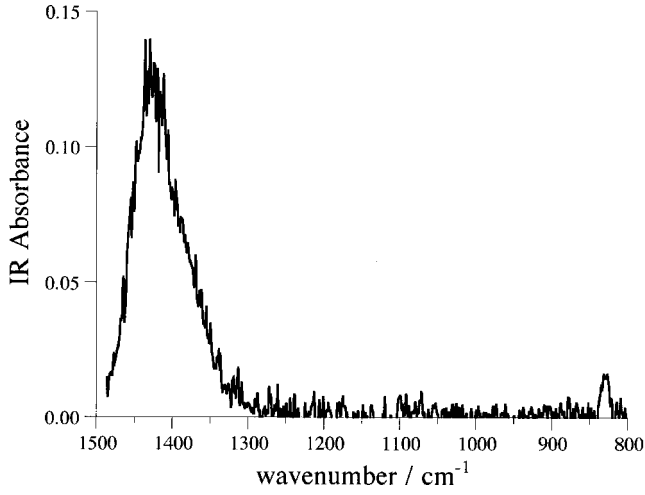

Figure 16. FTIR spectrum of polydisperse $NaNO_3$ particles in air (297 K; 2% RH; 52 m path length; 1 cm^{-1} resolution). The total particle number concentration was approximately 10^5 particles cm^3, with a geometric mean diameter of 362 nm (standard geometric deviation of 1.34) based on particle number. Water absorption lines have been subtracted.

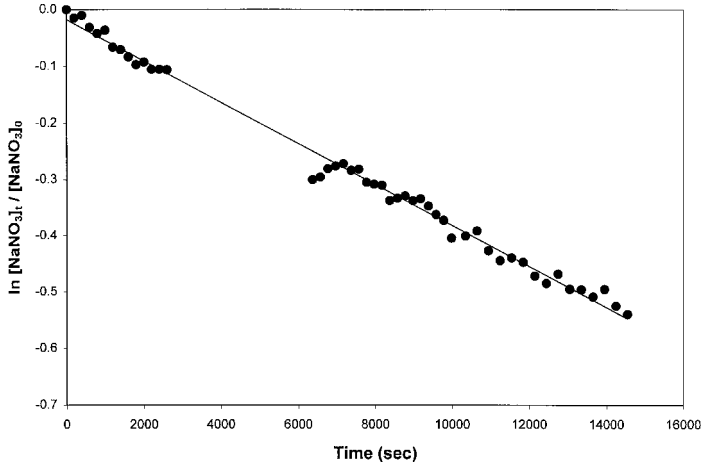

Figure 17. Temporal depletion of polydisperse $NaNO_3$ particles by wall deposition in the chamber (197 K; 2% RH; 636 Torr total pressure). The infrared absorption signal of $NaNO_3$ particles (1350–1500 cm^{-1}) was monitored as a function of time, and the first-order loss rate was obtained from the slope.

diffusion processes which lead to faster transport to, and removal at, the walls, as well as to coagulation into larger particles (Hinds 1982, McMurry and Rader 1985). Gravitational settling is expected to become dominant only at particle sizes of 1μm or greater (Hinds 1982), which are out of the range of the scanning mobility particle sizing system. In the range 0.1–1.0 μm, electrostatic forces due to build-up of charge on the walls of Teflon chambers are the dominant cause of loss of charged particles and probably play some role in this halocarbon-wax-coated chamber as well (McMurry and Rader 1985).

The wall deposition of polydisperse $NaNO_3$ particles was also monitored by FTIR spectrometry using the decline in condensed nitrate IR absorbance bands, shown in

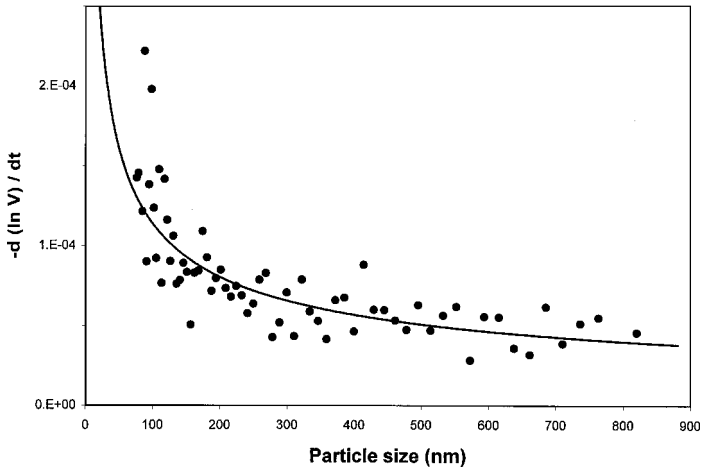

Figure 18. Size-dependent particle loss rates for $NaNO_3$ particles in the chamber measured with the SMPS system. First-order loss rates were taken from the slopes of temporal depletion of the particle numbers at 0, 0.07, 2.4 and 2.5 h respectively. The solid curve is provided as a guide to the eye only.

figure 16. The absorption in the 1350–1500 cm^{-1} range was used to follow the loss of these particles. Figure 17 shows that the loss was a first-order process characterized by $k_{wall} = (3.51 \pm 0.24) \times 10^{-5}\ s^{-1}$. This represents essentially a volume-weighted average of all particle sizes and their differential loss rates. Figure 18 shows the $NaNO_3$ particle loss rates measured using SMPS as a function of size. Loss rates for the larger particles which are expected to dominate the IR absorption are in the range of $5 \times 10^{-5}\ s^{-1}$, consistent with that measured using FTIR spectrometry.

The sampling rate of the scanning mobility particle sizer ranged between 0.2 and 0.6 l min^{-1}. Constant sampling during an experiment would thus cause a pressure loss in the chamber of at least 15 Torr h^{-1}. In addition to altering the conditions of the experiment, this pressure loss also disturbs the flow rates through the electrostatic classifier in the SMPS system, resulting in a false time-dependent shift to smaller particle sizes. To avoid these problems, particles in the chamber were sampled regularly, but not continuously, in most experiments and the flow rates were reset for each sampling period.

Gaseous reactants and aerosol streams were typically added at opposite ends of the chamber to avoid 'pre-reactions' between concentrated gas reactant and aerosol streams during fills. Particles which were visible to the eye when illuminated by the DOAS beam (diameter, 400 nm or greater) appeared to be well mixed after about 10–15 min in the chamber. At shorter times, laminae of particle-rich and particle-poor air could be seen within the illuminated area. Gas mixing from one end of the chamber to the other should be at least as fast as particle mixing because of faster gas diffusion rates. In general, mixing times are short compared with the time frame of the experiments. Furthermore, changes due to mixing along the length of the chamber do not affect the long-path optical measurements because the orientation of the light paths causes averaging in this direction. Thus, the main unwanted effect of slow mixing on FTIR and DOAS measurements is to obscure the exact starting time of an experiment. However, the API–MS and particle size measurements are point sampling techniques and may therefore be used to detect initial concentration changes due to mixing processes.

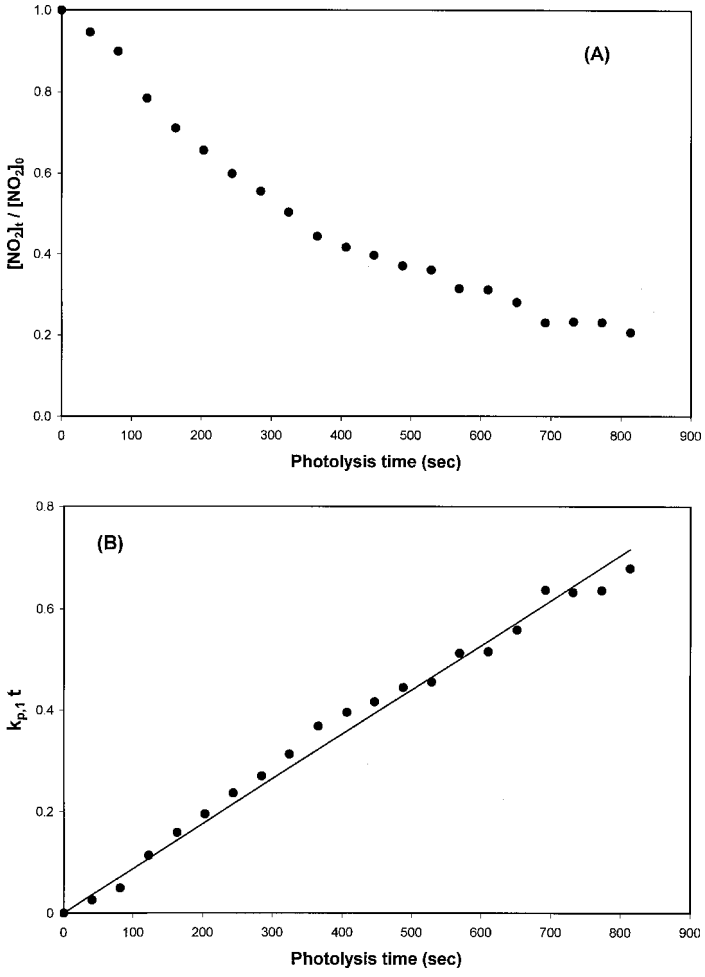

Figure 19. (*a*) Loss of NO_2 as a function of photolysis time using FTIR spectrometry to follow the loss of NO_2. NO_2 was photolysed by black lamps (16 tubes) in nitrogen (initial concentration of NO_2 of 5 ppm in argon at 492 Torr at 299 K and 0.2% RH); (*b*) plot of the right-hand side of equation (42) using the measured decay of NO_2 as a function of photolysis time. The slope gives the photolysis rate constant of interest, namely k_p.

The chamber photolysis systems were tested and characterized by separate experiments with NO_2 and ozone. The photolysis rate k_p for NO_2 in nitrogen was measured in two sets of experiments using black lamps and mercury lamps. The NO_2 photolysis rate is a measure of the total light intensity of each source in the region below 430 nm (Holmes *et al.* 1973):

$$NO_2 + h\nu \xrightarrow{k_p} O(^3P) + NO. \tag{10}$$

Secondary reactions of O and NO to remove or form NO_2 must be considered in the kinetics:

$$NO_2 + O \xrightarrow{k_{39}} O_2 + NO, \tag{39}$$

$$NO_2 + O + M \xrightarrow{k_{40}} NO_3 + M, \tag{40}$$

$$NO + O + M \xrightarrow{k_{41}} NO_2 + M. \tag{41}$$

Assuming that no O_2 is present, the photolysis rate constant k_p is derived using recommended rate constants for the other reactions (De More *et al.* 1997) and the equation (Holmes *et al.* 1973)

$$k_p\, t = \frac{1}{2}\left[\left(1 + \frac{k_{40}[M]}{k_{39}} - \frac{k_{41}[M]}{k_{39}}\right)\ln\left(\frac{[NO_2]_0}{[NO_2]_t}\right) + \frac{k_{41}[M]}{k_{39}}\left(\frac{[NO_2]_0}{[NO_2]_t} - 1\right)\right]. \tag{42}$$

Experimental data for NO_2 losses during illumination of 5 ppm NO_2 in argon by 16 black lamps are shown in figure 19(*a*), and plotted in the form of equation (42) in figure 19(*b*). The photolysis rate constant $k_p = (8.49 \pm 0.21) \times 10^{-4}\ s^{-1}$ corresponds to a ground-level atmospheric value at a zenith angle of about 80°, near sunrise (Brauers and Hofzumahaus 1992, Lantz *et al.* 1996, Kraus and Hofzumahaus 1998).

The loss of ozone by photolysis at 254 nm was also measured in both dry and humid nitrogen atmospheres using low-pressure mercury lamps. The first-order rate constant for ozone photolysis in dry N_2 for four ultraviolet lamps was measured, which represents a combination of photolysis and some regeneration by the reaction of $O(^3P)$ with O_2. A kinetic model of the system was used to extract the initial photolysis rate constant as $k_p = 8 \times 10^{-4}\ s^{-1}$. This rate is about 110 times higher than the real atmosphere at zenith angle of 60°. The loss of ozone is about five times higher in the humid chamber than in the dry chamber because of the reaction of $O(^1D)$ with water to generate OH, which destroys O_3 through well known secondary chemistry. The specific location of the lamps on top of the chamber did not impact the photolysis rates, probably owing to the high reflectivity of the inside of the chamber.

4.5. *Typical experimental results*

4.5.1. *The generation of Cl_2 from the photochemical reaction of O_3 with sea salt particles*

As described earlier in this article, the field studies of Keene *et al.* (1990) and the laboratory studies of Zetzsch and Behnke (1993) and Behnke *et al.* (1995) suggested that a search should be made for photochemical reactions involving ozone and sea salt particles which could generate Cl_2 or other photolysable halogen-containing gas products. A study of ozone reactivity in the presence of sea salt aerosol in either the solid or the liquid phase was therefore launched (Oum *et al.* 1998a).

FTIR and differential optical absorption lamp (I_0) spectra were taken in the evacuated chamber after pumping for at least 3 h. The chamber is filled with ultrahigh-purity nitrogen to about 600 Torr, including in some experiments enough water vapour to achieve a desired high humidity after all reactants are added. Spectral changes due to water vapour were recorded by FTIR spectrometry.

A synthetic sea salt solution (1.0% w/w) was atomized, and the resultant aerosol stream dried (and neutralized) to generate solid sea salt particles. The particle output was characterized using SMPS before the aerosol stream is redirected into the chamber. Once in the chamber, solid sea salt particles take up water vapour and deliquesce in high-humidity environments (75% or more RH). While this causes the particle surface area to increase rapidly, it is probably more significant that the phase change opens up the entire aerosol volume to participate in liquid-phase reactions. FTIR and differential optical absorption spectra were again recorded.

Gaseous reactants were added to the aerosol chamber after particles because the gas addition process is faster, thus minimizing uncertainties in experimental start

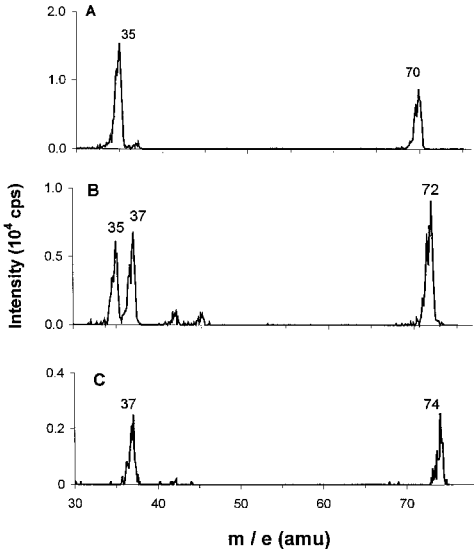

Figure 20. MS–MS scans (40 scans coadded) of the peaks at (*a*) $m/e = 70$, (*b*) $m/e = 72$ and (*c*) $m/e = 74$ after irradiation of O_3 at a initial concentration of 14 ppm for 10 min and a polydisperse sea salt aerosol in air at 86% RH and 298 K. (Reprinted with permission from K. W. Oum, M. J. Lakin, D. O. De Haan, T. Brauers and B. J. Finlayson-Pitts, 1998, *Science*, **279**, 74. Copyright 1998 American Association for Advancement of Science. Readers may view, browse, and/or download this material for temporary copying purposes only, provided these uses are for noncommercial personal purposes. Except as provided by law, this material may not be further reproduced, distributed, transmitted, modified, adapted, performed, displayed, published, or sold in whole or in part, without prior written permission from AAAS.)

times. Ozone was added to the chamber to attain initial concentrations between 0.8 and 14 ppm. Meanwhile, the flow paths on the particle equipment were adjusted for underpressure sampling to allow measurement of particle size distribution in the chamber. As the gaseous reactant was added, both long-path optical instruments record data at matched intervals, and initial chamber mass spectra were measured by the API–MS. Ozone concentrations were followed by long-path FTIR spectrometry and DOAS, particle size distributions were monitored periodically by the SMPS system, and chlorine and other halogen products were detected by API–MS. Low-pressure mercury photolysis lamps (major output is at 254 nm) were then switched on for various periods. This wavelength was chosen as it generates $O(^1D)$ in the ozone photolysis but does not photolyse the molecular halogen compounds such as Cl_2 at a significant rate.

The production of chlorine was observed in these experiments and verified using the dual fragmentation capabilities of the tandem mass spectrometer, as shown in figure 20. Specific Cl_2 isotopes from the first quadrupole region can be further fragmented into Cl^- ions (negative-ion mode). The ion pairs 70–35, 72–35, 72–37 and 74–37 were all observed, confirming identification of Cl_2 as the product. Chlorine production was found to require the presence of liquid-phase sea salt aerosol, ozone and ultraviolet light (Oum *et al.* 1998a). Small amounts of chlorine production were observed from sea salt particles on the walls of the chamber from previous runs. However, when an aerosol-free experiment was performed using a Teflon bag as a chamber, no chlorine production was observed until aerosols were added and

photolysis initiated. No other gas-phase products were observed by DOAS, FTIR spectrometry or API–MS.

In summary, photochemical production of Cl_2 from the reaction of O_3 with aqueous sea salt particles has been observed in laboratory studies and may occur in air as well.

4.5.2. *Generation of Br_2 from the dark reaction of O_3 with NaBr and frozen sea water*

As discussed above, there is ample evidence for the importance of bromine atoms in the chemistry of surface air in the Arctic at polar sunrise. While there are autocatalytic mechanisms which will regenerate photochemically active bromine compounds from sea salt reactions, the initiation step for such cycles is not known. Studies of the reactions of frozen sea water, as well as NaBr aerosols at room temperature, were therefore undertaken in this laboratory to elucidate the initiation reactions.

Bulk solutions of synthetic sea water similar to those used to generate the aerosol particles in the studies described in section 4.5.1 were frozen at $-80\ ^{\circ}C$ and exposed to O_3 in the dark (Oum *et al.* 1998b). The production of Br_2 was observed, in contrast with the room-temperature reaction of synthetic sea salt particles where Cl_2 production did not occur in the dark (Oum *et al.* 1998a). (However, if Br_2 was generated in the aerosol chamber experiments, it would not have been detectable because of the small total concentrations of available bromide in sea water). These experiments suggest, then, that the reaction of O_3 in the dark during the winter at the frozen ocean surface produces Br_2 and that this then photolyses at polar sunrise, initiating the autocatalytic destruction of ozone.

We have also observed production of gaseous Br_2 in the dark reaction of O_3 with NaBr aerosols at relative humidities above their deliquescence point. Figure 21, for example, shows the increase in signal at $m/e = 160$ due to Br_2 when O_3 was added to an NaBr aerosol at a RH in the range 83–85%. The identification of Br_2 was confirmed by the MS–MS of the parent peaks at $m/e = 158$, 160 and 162. Rapid formation of Br_2 is observed, consistent with the recent report of Br_2 as a product of the oxidation of bromide in NaBr and NaBr–NaCl mixtures by O_3 at room temperature (Hirokawa *et al.* 1998). Although the aim of these initial experiments was not to quantify the yield of Br_2, the maximum signal in figure 21 corresponds to about 30 ppb Br_2. For this polydisperse NaBr aerosol, this corresponds to oxidation of most of the bromide in the particles, at which point the generation of Br_2 ceases.

The mechanism of production of Br_2 in these systems is probably analogous to the well known reaction of ozone with bromide in bulk aqueous solutions. Ozone is known to oxidize aqueous Br^- readily at room temperature, forming OBr^- and HOBr (for example Taube (1942), von Gunten and Hoigné (1994) and von Gunten and Oliveras (1998)), and the same mechanism may occur in the quasi-liquid layer (for example Conklin and Bales (1993) and Brimblecombe and Conklin (1996)) on the ice surface:

$$O_3 + Br^- \rightarrow OBr^- + O_2, \tag{43}$$

$$OBr^- + H^+ \leftrightarrow HOBr, \tag{44}$$

$$HOBr + Br^- \rightarrow Br_2 + OH^-. \tag{45}$$

The reaction of O_3 with Cl^- is about five orders of magnitude slower than with Br^- (Hoigné *et al.* 1985), so that the same dark oxidation reaction is not significant for chloride.

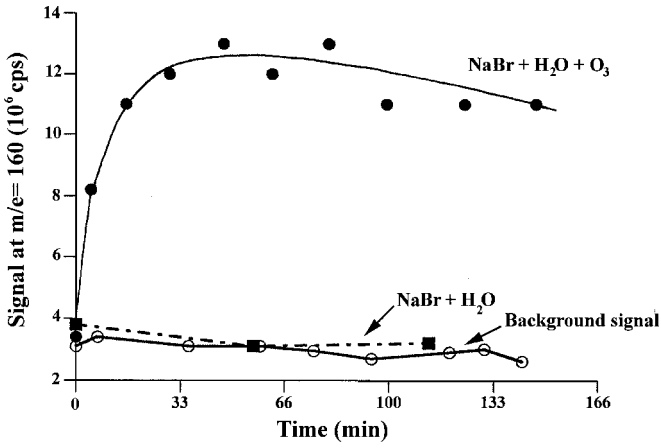

Figure 21. Relative intensity of MS peak at $m/e = 160$ due to Br_2 during the dark reaction of O_3 at an initial concentration of about 6 ppm with NaBr aerosol particles at 83–85% RH and 297 K.

In the case of frozen sea water, the reaction of HOBr with Cl^- also occurs:

$$HOBr + Cl^- \rightarrow BrCl + OH^- . \quad (46)$$

Indeed, as discussed by Oum *et al.* (1998b), reaction (46) of HOBr with Cl^- is expected to predominate over that with Br^- in sea water because of the high concentrations of chloride. However, BrCl rapidly hydrolyses in solution to form HOBr. In addition, it reacts with Cl^- to give $BrCl_2^-$ which hydrolyses to HOBr (Wang *et al.* 1994):

$$BrCl_2^- + H_2O \rightarrow HOBr + H^+ + 2Cl^- . \quad (47)$$

As a result, in spite of the higher concentrations of chloride ion in sea water, the chemistry is pushed towards Br_2 formation. It is also possible, and indeed likely, that this reaction sequence is also enhanced by enrichment of the surface layer of ice in bromide ion during freezing; however, this remains to be experimentally confirmed.

This proposed sea ice surface initiation mechanism is consistent with recent reports by Hopper *et al.* (1998) and Wagner and Platt (1998) in which the Arctic surface ozone destruction at polar sunrise and BrO production is reported to occur only over sea ice. It is also consistent with evidence from field studies (Impey *et al.* 1997) that photolysable bromine and chlorine compounds (which were not specifically identified) are formed at polar sunrise. Bromine compounds were reported at levels up to 38 ppt (as Br_2), and chlorine compounds up to 100 ppt (as Cl_2). Measured photolysable bromine compounds were positively correlated with O_3, as expected if reactions of O_3 such as those discussed above also led to the formation of these compounds.

In short, this new aerosol chamber, with its combination of FTIR spectroscopy, ultraviolet–visible DOAS and API–MS, has been shown to be a sensitive and useful instrument for the study of the heterogeneous chemistry of the marine boundary layer. We anticipate many other applications of this apparatus to the elucidation of heterogeneous reactions in the atmosphere.

5. Conclusions

Heterogeneous reactions of sea salt to give reactive halogen compounds in the troposphere appear increasingly likely to be important in marine areas, which includes many coastal urban areas. However, the detailed chemistry, particularly at a

molecular level, is still not well understood. Indeed, while compounds such as Cl_2 have now been specifically identified and measured in ambient air in coastal areas, even the overall chemistry leading to its formation is not known. Understanding such heterogeneous chemistry remains critically important for an accurate assessment of the chemistry of the troposphere on global to local scales.

Acknowledgments

We are grateful to the National Science Foundation, the US Department of Energy, the Joan Irvine Smith and Athalie R. Clarke Foundation and the University of California, Irvine, for support of the research described in this article. We have been fortunate to have a variety of talented scientists involved in much of the research discussed here, including Rainer Vogt, Sarka Langer and Sean Pemberton on the DRIFTS studies and Peter Beichert on the Knudsen cell studies. In addition, the development of the aerosol chamber was made possible through collaborations with John C. Hemminger, F. Sherwood Rowland and Darin Toohey, and through the technical skills of Phil Poyner, Lee Moritz, Jorg Meyer and Rick Fruchey. Helpful discussions and advice, particularly during design and testing of the aerosol chamber, from James N. Pitts, Jr, Roger Atkinson, Ernest Tuazon and Janet Arey, as well as experimental assistance from Matthew J. Lakin, Lisa Wingen, Dinh Quach, Michael Gebel, Yasmine Wadia, Weihong Wang and William S. Barney are also gratefully acknowledged. Finally, continuing stimulating scientific collaborations and discussions, covering a range from surface science to field studies, with John C. Hemminger, Chet Spicer, Carl Berkowitz and Elaine Chapman are gratefully acknowledged.

References

Alebic-Juretic, A., Cvitas, T., and Klasinc, L., 1992, *Ber. Bunsenges. phys. Chem.*, **96**, 493.
Aliwell, S. R., and Jones, R. L., 1998. *J. geophys. Res.*, **103**, 5719.
Andreae, M. O., and Crutzen, P. J., 1997, *Science*, **276**, 1052.
Allen, H. C., Laux, J. M., Vogt, R., Finlayson-Pitts, B. J., and Hemminger, J. C., 1996, *J. phys. Chem.*, **100**, 6371.
Ariya, P. A., Catoire, V., Sander, R., Niki, H., and Harris, G. W., 1997, *Tellus* B, **49**, 583.
Atkinson, R., 1997, *J. Phys. Chem. Ref. Data*, **26**, 215.
Atkinson, R., Aschmann, S. M., Arey, J., and Shorees, B., 1992, *J. geophys. Res.*, **97**, 6065.
Barrie, L. A., Bottenheim, J. W., Schnell, R. C., Crutzen, P. J., and Rasmussen, R. A., 1988, *Nature*, **334**, 138.
Behnke, W., George, C., Scheer, V., and Zetzsch, C., 1997, *J. geophys. Res.*, **102**, 3795.
Behnke, W., Kruger, H.-U., Scheer, V., and Zetzsch, C., 1991, *J. Aerosol Sci.*, **22**, S609; 1992, *ibid.*, **S23**, S933; 1993a, *Proceedings of the EUROTRAC Symposium '92*, edited by P. M. Borrell *et al.* (The Hague: SPB Academic), p. 565.
Behnke, W., Scheer, V., and Zetzsch, C., 1993b, *J. Aerosol Sci.*, **24**, S115; 1994, *ibid.*, **25**, S277; 1995, *Naturally-Produced Organohalogens*, edited by A. Grimwall and E. W. B. de Leer (Dordrecht: Kluwer), p. 375.
Behnke, W., and Zetsch, C.,1989a, *J. Aerosol Sci.*, **20**, 1167; 1989b, *Ozone in the Atmosphere*, edited by R. D. Bojkov and P. Fabian (Hampton, VA: Deepak), p. 519; 1990, *J. Aerosol Sci.*, **21**, S229.
Beichert, P., and Finlayson-Pitts, B. J., 1996, *J. phys. Chem.*, **100**, 15218.
Berko, H. N., McCaslin, P. C., and Finlayson-Pitts, B. J., 1991, *J. phys. Chem.*, **95**, 6951.
Blanchard, D. C., 1985, *J. geophys. Res.*, **90**, 961.
Bottenheim, J. W., Barrie, L. A., Atlas, E., Heidt, L. E., Niki, H., Rasmussen, R. A., and Shepson, P. B., 1990, *J. geophys. Res.*, **95**, 18555.
Bottenheim, J. W., Gallant, A. G. and Brice, K. A., 1986, *Geophys. Res. Lett.*, **13**, 113.
Brauers, T., and Hofzumahaus, A., 1992, *J. atmos. Chem.*, **15**, 269.

Brimblecombe , P., and Clegg , S. L., 1988, *J. atmos. Chem.*, **7**, 1; 1990, *Atmos. Environ.* A, **24**, 1945.

Brimblecombe , P., and Conklin , M. H., 1996, *Chemical Exchange Between the Atmosphere and Polar Snow*, NATO Advanced Study Institute Series, Vol. 143, edited by E. W. Wolff and R. C. Bales (Berlin: Springer), pp. 517–526.

Cadle , R. D., and Robbins , R. C., 1960, *Discuss, Faraday Soc.*, **30**, 155.

Cahill , T. A., Wilkinson , K., and Schnell , R., 1992, *J. geophys. Res.*, **97**, 14 513.

Caloz , F., Fenter , F. F., and Rossi, M. J., 1996, *J. phys. Chem.*, **100**, 7494.

Caloz , F., Fenter , F. F., Tabor , K. D., and Rossi, M. J., 1997, *Rev. scient. Instrum.*, **68**, 3172.

Chameides , W. L. and Stelson , A. W., 1992, *J. geophys. Res.*, **97**, 20 565.

Chance , K., 1998, *Geophys Res. Lett.*, **25**, 3335.

Chung , T. T., Dash , J., and O'Brien , R. J., 1978, *Proceedings of the Ninth International Congress on Electron Microscopy*, Toronto, 1978 (Toronto: Microscopical Society of Canada), p. 440.

Cicerone , R. J., 1981, *Rev. Geophys. Space Phys.*, **19**, 123.

Clegg , S. L., and Brimblecombe , P., 1985, *Atmos. Environ.*, **19**, 465; 1986, *ibid.*, **20**, 2483; 1988a, *ibid.*, **22**, 91; 1988b, *ibid.*, **22**, 117; 1990, *J. phys. Chem.*, **94**, 5369.

Cofer , W. R., III, Stevens , R. K., Winstead , E. L., Pinto , J. P., Sebacher , D. I., Abdulraheem , M. Y., Al-Sahafi , M., Mazurek , M. A., Rasmussen , R. A., Cahoon , D. R., and Levine , J. S., 1992, *J. geophys. Res.*, **97**, 14 521.

Conklin , M. H., and Bales , R. C., 1993, *J. geophys. Res.*, **98**, 16 851.

Dai, D. J., Peters , S. J., and Ewing , G. E., 1995, *J. phys. Chem.*, **99**, 10 299.

Dai, Q., Hu , J., and Salmeron , M., 1997, *J. phys. Chem.* B, **101**, 1994.

Daum , P. H., Al-Sunaid , A., Busness , K. M., Hales , J. M., and Mazurek , M., 1993, *J. geophys. Res.*, **98**, 16 809.

Davies , J. A., and Cox , R. A., 1998, *J. phys. Chem.* A, **102**, 7631.

De Haan , D. O., and Finlayson -Pitts , B. J., 1997, *J. Phys. Chem.* A, **101**, 9993.

De More , W. B., Sander , S. P., Golden , D. M., Hampson , R. F., Kurylo , M. J., Howard , C. J., Ravishankara , A. R., Kolb , C. E., and Molina , M. J., 1997, *Chemical Kinetics and Photochemical Data for Use in Stratospheric Modeling*, NASA–JPL Publication 97–4 (Pasadena, CA: Jet Propulsion Laboratory, CalTech).

Donahue , N. M., Kroll , J. H., Anderson , J. G., and Demerjian , K. L., 1998, *Geophys. Res. Lett.*, **25**, 59.

Dorn, H.-P., Brandenburger , U., Brauers , T., Hausmann , M., and Ehhalt , D. H., 1996, *Geophys. Res. Lett.*, **23**, 2537.

Eisele , F. L., Mount , G. H., Fehsenfeld , F. C., Harder , J., Marovich , E., Parrish , D. D., Roberts , J. and Trainer , M., 1994, *J. geophys. Res.*, **99**, 18 605.

Fan , S.-M., and Jacob , D. J., 1992, *Nature*, **359**, 522.

Fenter , F. F., Caloz , F., and Rossi, M. J., 1994, *J. phys. Chem.*, **98**, 9801; 1996, *ibid.*, **100**, 1008; 1997, *Rev. scient. Instrum.*, **68**, 3180.

Ferek , R. J., Hobbs , P. V., Herring , J. A., Laursen , K. K., Weiss , R. E., and Rasmussen , R. A., 1992, *J. Geophys. Res.*, **97**, 14 483.

Finlayson -Pitts , B. J., 1983, *Nature*, **306**, 676; 1993, *Res. Chem. Intermed.*, **19**, 235.

Finlayson -Pitts , B. J., Ezell , M. J., and Pitts , J. N., Jr, 1989a, *Nature*, **337**, 241.

Finlayson -Pitts , B. J., and Johnson , S. N., 1988, *Atmos. Environ.*, **22**, 1107.

Finlayson -Pitts , B. J., Livingston , F. E., and Berko , H. N., 1989b, *J. phys. Chem.*, **93**, 4397; 1990, *Nature*, **343**, 622.

Finlayson -Pitts , B. J., and Pitts , J. N., Jr, 1986, *Atmospheric Chemistry: Fundamentals and Experimental Techniques* (New York: Wiley), and references therein; 1997, *Science*, **276**, 1045, and references therein.

Frenzel , A., Scheer , V., Sikorski , R., George , Ch., Behnke , W., and Zetzsch , C., 1998, *J. phys. Chem.* A; **102**, 1329.

George , Ch., Ponche , J. L., Mirabel , Ph., Behnke , W., Scheer , V., and Zetzsch , C., 1994, *J. phys. Chem.*, **98**, 8780.

Golden , D. M., Spokes , G. N., and Benson , S. W., 1973, *Angew. Chem., Int. Edn Engl.*, **12**, 534.

Gomer , T., Brauers , T., Heintz , F., Stutz , J., and Platt , U., 1995, *Manual of MFC* (University of Heidelberg).

Gong , S. L., Barrie , L. A., and Blanchet , J. P., 1997a, *J. geophys. Res.*, **102**, 3805.

GONG, S. L., BARRIE, L. A., PROSPERO, J. M., SAVOIE, D. L., AYERS, G. P., BLANCHET, J.-P., and SPACEK, L., 1997b, *J. geophys. Res.*, **102**, 3819.
GRAEDEL, T. E., and KEENE, W. C., 1995, *Global Biogeochem. Cycles*, **9**, 47.
HEBESTREIT, K., STUTZ, J., LURIA, M., PELEG, M., MATVEIV, V., ROZEN, D. and PLATT, U., 1998, *Ann. Geophys., Suppl. II*, **16**, C719.
HEMMINGER, J. C., 1999, *Int. Rev. phys. Chem.*, **18**, 387.
HINDS, W. C., 1982, *Aerosol Technology* (New York: Wiley), and references therein.
HIROKAWA, J., ONAKA, K., KAJII, Y., and AKIMOTO, H., 1998, *Geophys. Res. Lett.*, **25**, 2449.
HOFZUMAHAUS, A., ASCHMUTAT, U., HESSLING, M., HOLLAND, F., and EHHALT, D. H, 1996, *Geophys. Res. Lett.*, **23**, 2541.
HOIGNÉ, J., BADER, H., HAAG, W. R., and STAEHELIN, J., 1985, *Water Res.*, **19**, 993.
HOLMES, J. R., O'BRIEN, R. J., CRABTREE, J. H., HECHT, T. A., and SEINFELD, J. H., 1973, *Environ. Sci. Technol.* **7**, 519.
HOLTON, J. R., HAYNES, P. H., MCINTYRE, M. E., DOUGLASS, A. R., ROOD, R. B., and PFISTER, L., 1995, *Rev. Geophys.*, **33**, 403.
HOPPER, J. F., BARRIE, L. A., SILIS, A., HART, W., GALLANT, A. J., and DRYFHOUT, H., 1998, *J. geophys. Res.*, **103**, 1481.
HOV, O., 1985, *Atmos. Environ.* **19**, 471.
IKEGAMI, M., OKADA, K., ZAIZEN, Y., and MAKINO, Y., 1994, *Tellus* B, **46**, 142.
IMPEY, G. A., SHEPSON, P. B., HASTIE, D. R., BARRIE, L. A., and ANLAUF, K. G., 1997, *J. Geophys. Res.*, **102**, 16005.
JOBSON, B. T., NIKI, H., YOKOUCHI, Y., BOTTENHEIM, J., HOPPER, F., and LEAITCH, R., 1994, *J. Geophys. Res.*, **99**, 25355.
JOHNSON, E. R., 1970, *The Radiation-Induced Decomposition of Inorganic Molecular Ions* (New York: Gordon and Breach).
JUNGE, C. E., 1956, *Tellus*, **8**, 127.
JUNKERMANN, W., and IBUSUKI, T., 1992, *Atmos. Environ.* A, **26**, 3099.
KARLSSON, R., and LJUNGSTRÖM, E., 1995, *J. Aerosol Sci.*, **26**, 39.
KEENE, W. C., 1995, *Naturally-Produced Organohalogens*, edited by A. Grimvall and E. W. B. de Leer (Dordrecht: Kluwer), p. 363.
KEENE, W. C., JACOB, D. J., and FAN, S.-M., 1996, *Atmos. Environ.*, **30**, 1.
KEENE, W. C., MABEN, J. R., PSZENNY, A. A. P., and GALLOWAY, J. N., 1993, *Environ. Sci. Technol.*, **27**, 866.
KEENE, W. C., PSZENNY, A. A. P., and ERICKSON, D. J., 1998a, *J. Aerosol Sci.*, **29**, 339.
KEENE, W. C., PSZENNY, A. A. P., JACOB, D. J., DUCE, R. A., GALLOWAY, J. N., SCHULTZ-TOKOS, J. J., SIEVERING, H., and BOATMAN, J. F., 1990, *Global Biogeochem. Cycles*, **4**, 407.
KEENE, W. C., SANDER, R., PSZENNY, A. A. P., VOGT, R., CRUTZEN, P. J., and GALLOWAY, J. N., 1998b, *J. Aerosol Sci.*, **29**, 339.
KEENE, W. C., and SAVOIE, D., 1998, *Geophys. Res. Lett.*, **25**, 2181.
KRAUS, A., and HOFZUMAHAUS, A., 1998, *J. Atmos. Chem.*, **31**, 161.
LAD, R. A., 1968, *Surf. Sci.*, **12**, 37.
LANGER, S., PEMBERTON, R. S., and FINLAYSON-PITTS, B. J., 1997, *J. phys. Chem.* A, **101**, 1277.
LANTZ, K. O., SHETTER, R. E., CANTRELL, C. A., FLOCKE, S. J., CALVERT, J. G., and MADRONICH, S., 1996, *J. geophys. Res.*, **101**, 14613.
LAUX, J. M., FISTER, T. F., FINLAYSON-PITTS, B. J., and HEMMINGER, J. C., 1996, *J. phys. Chem.*, **100**, 19891.
LAUX, J. M., HEMMINGER, J. C., and FINLAYSON-PITTS, B. J., 1994, *Geophys. Res. Lett.*, **21**, 1623.
LEIGHTON, P. A., 1961, *Photochemistry of Air Pollution* (New York: Academic Press).
LEU, M.-T., TIMONEN, B. S., and KEYSER, L. F., 1997, *J. phys. Chem.* A., **101**, 278.
LEU, M.-T., TIMONEN, R. S., KEYSER, L. F., and YUNG, Y. L., 1995, *J. Phys. Chem.*, **99**, 13203.
LIVINGSTON, F. E., and FINLAYSON-PITTS, B. J., 1991, *Geophys. Res. Lett.*, **18**, 17.
LOWENTHAL, D. H., BORYS, R. D., ROGERS, C. F., CHOW, J. C., STEVENS, R. K., PINTO, J. P., and ONDOV, J. M., 1993, *Geophys. Res. Lett.*, **20**, 691.
MABEN, J. R., KEENE, W. C., PSZENNY, A. A. P., and GALLOWAY, J. N., 1995, *Geophys. Res. Lett.*, **22**, 3513.
MAMANE, Y., and GOTTLIEB, J., 1990, *J. Aerosol Sci.*, **21**, S225.
MARSH, A. R. W., and MCELROY, W. J., 1985, *Atmos. Environ.*, **19**, 1075.
MARTENS, C. S., WESOLOWSKI, J. J., HARRISS, R. C., and KAIFER, R., 1973, *J. geophys. Res.*, **78**, 8778.
MCCARTHY, M. I., PETERSON, K. A., and HESS, W. P., 1996, *J. phys. Chem.*, **100**, 6708.

McConnell, J. C., Henderson, G. S., Barrie, L., Bottenheim, J., Niki, H., Langford, C. H., and Templeton, E. M. J., 1992, *Nature*, **355**, 150.
McInnes, L. M., Covert, D. S., Quinn, P. K., and Germani, M. S., 1994, *J. geophys. Res.*, **99**, 8257.
McMurry, P. H., and Rader, D. J., 1985, *Aerosol Sci. Technol.*, **4**, 249.
Michelangeli, D. V., Allen, M., and Yung, Y. L., 1991, *Geophys. Res. Lett.*, **18**, 673.
Mochida, M., Akimoto, H., van den Bergh, H., and Rossi, M. J., 1998, *J. phys. Chem.* A, **102**, 4819.
Mouri, H., and Okada, K., 1993, *Geophys. Res. Lett.*, **20**, 49.
Moyers, J. L., and Duce, R. A., 1972, *J. geophys. Res.*, **77**, 5330.
Msibi, I. M., Li, Y., Shi, J. P., and Harrison, R. M., 1994, *J. atmos. Chem.*, **18**, 291.
Niki, H., and Becker, K. H., 1993, *The Tropospheric Chemistry of Ozone in the Polar Regions*, NATO Advanced Study Institute Series, Vol. 7 (Berlin: Springer), pp. 1–416.
O'Dowd, C. D., Smith, M. H., Consterdine, I. E., and Lowe, J. A., 1997, *Atmos. Environ.*, **31**, 73.
Oltmans, S. J. and Komhyr, W. D., 1986, *J. geophys. Res.*, **91**, 5229.
Oum, K. W., Lakin, M. J., De Haan, D. O., Brauers, T., and Finlayson-Pitts, B. J., 1998a, *Science*, **279**, 74.
Oum, K. W., Lakin, M. J., and Finlayson-Pitts, B. J., 1998b, *Geophys. Res. Lett.*, **25**, 3923.
Parungo, F., Kopcewicz, B., Nagamoto, C., Schnell, R., Sheridan, P., Zhu, C., and Harris, J., 1992, *J. geophys. Res.*, **97**, 15867.
Paulson, S. E., and Orlando, J. J., 1996, *Geophys. Res. Lett.*, **23**, 3727.
Paulson, S. E., Sen, A. D., Liu, P., Fenske, J. D., and Fox, M. J., 1997, *Geophys. Res. Lett.* **24**, 3193.
Platt, U., 1994, *Air Monitoring by Spectroscopic Techniques*, Chemical Analysis Series, Vol. 127, edited by M. W. Sigrist (New York: Wiley), pp. 27–84.
Platt, U., and Hausmann, M., 1994, *Res. Chem. Intermed.*, **20**, 557.
Platt, U., LeBras, G., Poulet, G., Burrows, J. P., and Moortgat, G., 1990, *Nature*, **348**, 147.
Peters, S. J., and Ewing, G. E., 1996, *J. phys. Chem.*, **100**, 14093; 1997, *Langmuir*, **13**, 6345.
Pósfai, M., Anderson, J. R., Buseck, P. R., and Sievering, H., 1995, *J. geophys. Res.*, **100**, 23063.
Pszenny, A. A. P., Keene, W. C., Jacob, D. J., Fan, S., Maben, J. R., Zetwo, M. P., Springer-Young, M., and Galloway, J. N., 1993, *Geophys. Res. Lett.*, **20**, 699.
Quinlan, M. A., Reihs, C. M., Golden, D. M., and Tolbert, M. A., 1990, *J. phys. Chem.*, **94**, 3255.
Ravishankara, A. R., 1997, *Science*, **276**, 1058.
Reid, J. S., Flocchini, R. G., Cahill, T. A., and Ruth, R. S., 1994, *Atmos. Environ.*, **28**, 1699.
Richter, A., Wittrock, F., Eisinger, M., and Burrows, J. P., 1998, *Geophys. Res. Lett.*, **25**, 2683.
Robbins, R. C., Cadle, R. D., and Eckhardt, D. L., 1959, *J. Metals*, **16**, 53.
Rudolph, J., Koppmann, R., and Plass-Dülmer, Ch., 1996, *Atmos. Environ.*, **30**, 1887.
Sander, R., and Crutzen, P. J., 1996, *J. geophys. Res.*, **101**, 9121.
Schroeder, W. H., and Urone, P., 1974, *Environ. Sci. Technol.*, **8**, 756.
Schweitzer, F., Mirabel, P., and George, C., 1998, *J. phys. Chem.*, **102**, 3942.
Seisel, S., Caloz, F., Fenter, F. F., van den Bergh, H. and Rossi, M. J. 1997, *Geophys. Res. Lett.*, **24**, 2757.
Shaw, G. E., 1991, *J. Geophys. Res.*, **96**, 22369.
Sheridan, P. J., Schnell, R. C., Hofmann, D. J., Harris, J. M., and Deshler, T., 1992, *Geophys. Res. Lett.*, **19**, 389.
Shindo, H., Ohashi, M., Tateishi, O., and Seo, A., 1997, *J. chem. Soc., Faraday Trans.*, **93**, 1169.
Sievering, H., Boatman, J., Gorman, E., Kim, Y., Anderson, L., Ennis, G., Luria, M., and Pandis, S., 1992, *Nature*, **360**, 571.
Sievering, H., Gorman, E., Ley, T., Pszenny, A., Springer-Young, M., Boatman, J., Kim, Y., Nagamoto, C., and Wellman, D., 1995, *J. geophys. Res.*, **100**, 23075.
Singh, H. B., Gregory, G. L., Anderson, B., Browell, E., Sachse, G. W., Davis, D. D., Crawford, J., Bradshaw, J. D., Talbot, R., Blake, D. R., Thornton, D., Newell, R., and Merrill, J., 1996a, *J. geophys. Res.*, **101**, 1907.

SINGH, H. B., and KASTING, J. F., 1988, *J. atmos. Chem.*, **7**, 261.
SINGH, H. B., THAKUR, A. N., CHEN, Y. E., and KANAKIDOU, M., 1996b, *Geophys. Res. Lett.*, **23**, 1529.
SOLBERG, S., SCHMIDBAUER, N., SEMB, A., STORDAL, F. and HOV, Ø., 1996, *J. atmos. Chem.*, **23**, 301.
SPICER, C. W., 1994, *Environ. Sci. Technol.*, **28**, A378.
SPICER, C. W., CHAPMAN, E. G., FINLAYSON-PITTS, B. J., PLASTRIDGE, R. A., HUBBE, J. M., FAST, J. D., and BERKOWITZ, C. M., 1998, *Nature*, **394**, 353.
STEVENS, R., PINTO, J., MAMANE, Y., ONDOV, J., ABDULRAHEEM, M., ALMAJED, N., SADEK, M., COFER, W., ELLENSON, W., and KELLOGG, R., 1993, *Water Sci. Technol.*, **27**, 223.
STURGES, W. T., 1989, *Atmos. Environ.*, **23**, 1167.
STUTZ, J., EZELL, M. J., EZELL, A. A., and FINLAYSON-PITTS, B. J., 1998, *J. phys. Chem.* A, **102**, 8510.
SVERDRUP, G. M., and KUHLMAN, M. R., 1980, *Atmospheric Pollution*, Proceedings of the 14th International Colloquium, Paris, 5–8 May, 1980, Studies in Environmental Science, Vol. 8, edited by M. M. Benarie (Amsterdam: Elsevier), p. 245.
TANG, I. N., and MUNKELWITZ, H. R., 1984, *J. Colloid. Interface Sci.*, **98**, 430; 1993, *Atmos. Environ.* A, **27**, 467.
TANG, I. N., MUNKELWITZ, H. R., and DAVIS, J. G., 1977, *J. Aerosol Sci.*, **8**, 149; 1978, *ibid.*, **9**, 505.
TANG, I. N., MUNKELWITZ, H. R., and LEE, J. H., 1988, *Atmos. Environ.*, **22**, 2579.
TANG, I. N., TRIDICO, A. C., and FUNG, K. H., 1997, *J. geophys. Res.*, **102**, 23 269.
TANG, T., and MCCONNELL, J. C., 1996, *Geophys. Res. Lett.*, **23**, 2633.
TAUBE, H., 1942, *J. Am. chem. Soc.*, **64**, 2468.
TEN BRINK, H. M., 1998, *J. Aerosol Sci.*, **29**, 57.
TIMONEN, R. S., CHU, L. T., LEU, M.-T., and KEYSER, L. F., 1994, *J. phys. Chem.*, **98**, 9509.
TUCKERMANN, M., ACKERMANN, R., GÖLZ, C., LORENZEN-SCHMIDT, H., SENNE, T., STUTZ, J., TROST, B., UNOLD, W., and PLATT, U., 1997, *Tellus* B, **49**, 533.
VOGT, R., CRUTZEN, P. J., and SANDER, R., 1996a, *Nature*, **383**, 327.
VOGT, R., ELLIOTT, C., ALLEN, H. C., LAUX, J. M., HEMMINGER, J. C., and FINLAYSON-PITTS, B. J., 1996b, *Atmos. Environ.*, **30**, 1729.
VOGT, R., and FINLAYSON-PITTS, B. J., 1994a, *J. phys. Chem.*, **98**, 3747; 1994b, *Geophys. Res. Lett.*, **21**, 2291; 1995a, *J. phys. Chem.*, **99**, 13052; 1995b, *J. phys. Chem.*, **99**, 17269.
VON GUNTEN, U., and HOIGNÉ, J., 1994, *Environ. Sci. Technol.*, **28**, 1234.
VON GUNTEN, U., and OLIVERAS, Y., 1998, *Environ. Sci. Technol.*, **32**, 63.
WAGNER, T., and PLATT, U., 1998, *Nature*, **395**, 486.
WANG, T. X., KELLEY, M. D., COOPER, J. N., BECKWITH, R. C., and MARGERUM, D. W., 1994, *Inorg. Chem.*, **33**, 5872.
WAYNE, R. P., POULET, G., BIGGS, P., BURROWS, J. P., COX, R. A., CRUTZEN, P. J., HAYMAN, G. D., JENKIN, M. E., LE BRAS, G., MOORTGAT, G. K., PLATT, U., and SCHINDLER, R. N., 1995, *Atmos. Environ.*, **29**, 2677.
WHITE, J. U., 1942, *J. opt. Soc. Am.*, **32**, 285; 1976, *ibid.*, **66**, 411.
WIEDENSOHLER, A., 1988, *J. Aerosol Sci.*, **19**, 387.
WINGENTER, O. W., KUBO, M. K., BLAKE, N. J., SMITH, JR., T. W., BLAKE, D. R., and ROWLAND, F. S., 1996, *J. geophys. Res.*, **101**, 4331.
WINKLER, T., GOSCHNICK, J., and ACHE, H. J., 1991, *J. Aerosol Sci.*, **22** (Suppl. 1), S605.
WOODCOCK, A. H., 1953, *J. Meteorol.*, **10**, 362; 1972, *J. geophys. Res.*, **77**, 5316.
WOODS, D. C., and CHUAN, R. L., 1983, *Geophys. Res. Lett.*, **10**, 1041.
WOODS, D. C., CHUAN, R. L., and ROSE, W. I., 1985, *Science*, **230**, 170.
WORLD METEOROLOGICAL ORGANIZATION, 1995, Global Ozone Research and Monitoring Project Report 37, February.
ZANGMEISTER, C. D., and PEMBERTON, J. E., 1998, *J. phys Chem.* B, **102**, 8950.
ZETZSCH, C., 1987, *Formation, Distribution and Chemical Transformation of Air Pollutants*, Monograph Vol. 104, edited by R. Zellner (New York: VCH), p. 187.
ZETZSCH, C., and BEHNKE, W., 1992, *Ber. Bunsenges. phys. Chem.*, **96**, 488; 1993, *The Tropospheric Chemistry of Ozone in the Polar Regions*, NATO Advanced Study Institute Series, Vol. 7, edited by H. Niki and K. H. Becker (Berlin: Springer), p. 291.
ZETZSCH, C., PFAHLER, G., and BEHNKE, W., 1988, *J. Aerosol Sci.*, **19**, 1203.